NASA CONTRACTOR REPORT

NASA CR-1443

NASA CR-1443


# TECHNIQUES FOR GENERATION OF CONTROL AND GUIDANCE SIGNALS DERIVED FROM OPTICAL FIELDS

*by H. Hemami, M. B. Kuhner, and L. T. Bashark*

*Prepared by*
OHIO STATE UNIVERSITY
Columbus, Ohio
*for Langley Research Center*

NATIONAL AERONAUTICS AND SPACE ADMINISTRATION • WASHINGTON, D. C. • OCTOBER 1969

NASA CR-1443

# TECHNIQUES FOR GENERATION OF CONTROL AND GUIDANCE SIGNALS DERIVED FROM OPTICAL FIELDS

By H. Hemami, M. B. Kuhner, and L. T. Bashark



Issued by Originator as Report RF 2421

Prepared under Grant No. NGR-36-008-076 by
OHIO STATE UNIVERSITY
Columbus, Ohio

for Langley Research Center

NATIONAL AERONAUTICS AND SPACE ADMINISTRATION

For sale by the Clearinghouse for Federal Scientific and Technical Information
Springfield, Virginia 22151 – CFSTI price $3.00

## FOREWORD

The study described in this report was conducted at the Communication and Control Systems Laboratory of The Ohio State University, and was supported by a grant from the National Aeronautics and Space Administration under Grant No. NGR-36-008-076. The NASA scientific officer was Mr. Thomas M. Walsh.

The study was performed under the supervision of H. Hemami. Special credit and acknowledgment is due Professor R. L. Cosgriff who initiated this study, and whose original thoughts and work have been invaluable to the progress of this study. Fruitful discussions with Professor C. Earl Warren and Mr. Thomas M. Walsh are gratefully acknowledged. The cooperation of Professor Robert E. Fenton, Acting Director of Communication and Control System Laboratory, is very much appreciated.

## ABSTRACT

A general transfer functional is derived for optical systems that relates the image intensity to the spatial autocorrelation of the aperture and temporal autocorrelation of the received signals. A simple method of detection of star images by cross-correlation techniques is developed. This cross-correlation requires certain image density characteristics that can be constructed by appropriate prefiltering of the signals. Synthesis of a class of such filters is carried out in a sequence of experiments, and the feasibility and performance of the filters are discussed.

Two methods of estimating the position of the star image are developed and their implications discussed. One method is based on generalized mean square error criterion and requires prefiltering and full knowledge of the star image intensity. For the second method partial knowledge about the star image is sufficient.

TABLE OF CONTENTS

FIGURES

FIGURES ( cont'd)

# I. INTRODUCTION

## 1.1 Scope of the Study

The performance of a star tracker, once the set of stars and consequently the background have been selected, largely depends on how accurate error signals can be generated. In turn, generation of accurate error signals depends on how well the misalignment of the tracker can be detected.

This report is primarily concerned with analytical and experimental investigation of methods of detection.

The analytical investigation must be carried out with several ends in mind.

One must be able to compare different existing star tracking systems. For efficient synthesis of a star tracker, trade offs between three elements involved in detection, namely, field of view, optical system,and detection system, must be derivable. This means, for a given field of view and a given optical system, one must be able to synthesize optimal detection schemes. Or, for a given optical system and detection scheme, one should be able to specify the types of stars and background that are optimal for effective tracking and so forth. Finally, if one looks far in advance one must consider adaptive systems in the sense that the tracker should be able to change its field of view from a given set of stars and background to another set. The system then must implement the necessary changes both in the optical and detection systems or preferably only in the detection system.

For this reason broad analytical tools will be developed that are applicable to the class of problems discussed.

The experimental investigation presented here is more restricted and is closely related to the detection scheme discussed in this report.

## 1.2 Brief Content of the Report and Main Results

In Part II, a general transfer functional is derived for the optical system. In addition to immediate application in this study, this transfer functional is intended to be useful in a variety of problems related to tracking:

1. It can be used for analysis of performance of optical systems (namely, studying effects of masks, wedges, and reticles) both in the object and image foci.

2. For a given optical system and given sensor it can be used to derive optimal processing of the sensor information.

3. It provides systematic synthesis methods in situations where a particular image intensity is desired for a pre-specified detection scheme.

In Part III, the problem of detection of the image is discussed. The problem is the detection of the location of the pertinent signals rather than detection of the existence of the signal. For this reason, the detection problem at hand is a parameter estimation problem where the parameters are the coordinates of the star image and the angle through which the image has rotated relative to some reference frame.

The parameter estimation problems can be handled by two distinct methods:

1. Cross-correlation techniques.

2. Sequential estimation techniques.

The first of these is considered in detail in Part III. A method of filtering is developed that would provide simple implementation of a cross-correlation technique. The method requires the star image intensity to have the shape of a cross. This image shaping can be achieved by appropriate pre-filtering of the field of view.

In Part IV these filters are empirically designed and their properties and implications are studied by simulation. The filters are constructed by a perpendicular mesh of wires. The effect of size and number of the wires on the image are experimentally investigated by both coherent and incoherent sources. These results are reported in Part IV.

Further experimental results are reported in Part V. These experiments are more concerned with the performance of the aforementioned spatial filters when the source is noncoherent. In particular the feasibility of utilizing the cross pattern in a sun tracking system is studied. Finally in Part V, the cross-correlation technique proposed in Part III is simulated, and a system resolution of 15 arc-second is obtained.

In Part VI a method for discrete sequential estimation of the star image position is developed. This method is based on a generalized mean square error minimization criterion. This method requires a special shape for star image intensity which can be achieved by pre-filtering techniques of Part II.

Advantages of this method are: minimal data for storage is required; most of the mathematical operations are linear, and the system has learning capability. The disadvantage of this technique is that exact knowledge of the star image intensity is required.

Since in some practical cases exact knowledge of the star image intensity is not available another discrete estimation technique is investigated in Part VII that requires partial knowledge about the star image intensity. This latter technique can be incorporated in star tracker system separately or in conjunction with the analog techniques of Part III. Finally the feasibility of this latter technique in pattern recognition problems concerned with acquisition of a star field rather tracking is investigated.

# II. TRANSFER FUNCTIONAL OF AN OPTICAL SYSTEM

## 2.1 Introduction

In this part, a general transfer functional is derived for an optical system that relates the intensity of the image to the spatial autocorrelation of the input signal--the field at the aperture--and the temporal autocorrelation of the field signal. In Section 2.2 a representation of a star field is discussed where the field is comprised of several monochromatic components.

The filtering of such a star field is discussed in Section 2.3.

The case where the power density spectrum of the field is continuous is discussed in Section 2.4, and the main result is derived.

To clarify some concepts, an example is included to demonstrate how this approach applies and what the computational implications are.

## 2.2 Representation of the Field

Let the light signal amplitude in the object focus of the optical system be represented by

$$E(x,y,t) = \sum_{i=1}^{n} A_i(x,y)\cos[w_i t + \beta_i(x,y)] \qquad (2.1)$$

That is, the field is the sum of several monochromatic components. Equation (2.1) can be conveniently written as an inner product

$$E(x,y,t) = \mathrm{Re}(F \cdot W) \quad = \mathrm{Re}(F^T W) \qquad (2.2)$$

where F is a column vector, and $F^T$ is its transpose - a row vector



4

$$F^T = [A_1(x,y)e^{j\beta_1(x,y)},\ A_2(x,y)e^{j\beta_2(x,y)},\ \ldots,$$
$$A_n(x,y)e^{j\beta n(x,y)}] \qquad (2.3)$$

and W is the following column vector

$$W = \begin{bmatrix} e^{jw_1 t} \\ e^{jw_2 t} \\ \cdot \\ \cdot \\ \cdot \\ e^{jw_n t} \end{bmatrix} \qquad (2.4)$$

## 2.3 Filtering of the Star Field by a Transparency

Let a transparency be inserted in the object focus. The transparency is described by an amplitude function $p(x,y)$ and a phase function $\alpha(x,y)$. Therefore the transparency is described by the complex transmittance function

$$P = p(x,y)e^{j\alpha(x,y)}$$

The phase function $\alpha(x,y)$ is a function of the thickness of the transparency and its index of refraction $n_1$. Let the thickness be $\gamma(x,y)$, then

$$\alpha(x,y) = \frac{\gamma(x,y)}{2\pi(n_1 - 1)} \qquad (2.5)$$

where in general $n_1$ is a function of $w_i$. The signal amplitude after the transparency, namely $E_1$, is given by

$$E_1 = \sum_{i=1}^{n} A_i(x,y)p(x,y)\cos(w_i t + \beta_i + \alpha_i) \qquad (2.6)$$

Alternately the column vector $F_1$ is given by

$$F_1 = \begin{bmatrix} f_{11} \\ \vdots \\ f_{1i} \\ \vdots \\ f_{1n} \end{bmatrix} = \begin{bmatrix} A_1(x,y)p(x,y)e^{j\beta_1(x,y)+j\alpha_1(x,y)} \\ \cdots\cdots\cdots\cdots\cdots\cdots \\ \cdots\cdots\cdots\cdots\cdots\cdots \\ A_n(x,y)p(x,y)e^{j\beta_n(x,y)+j\alpha_n(x,y)} \end{bmatrix} \qquad (2.7)$$

Let the complex image amplitude in the image focus be

$$F_2(u,v) = \begin{bmatrix} f_{21} \\ f_{22} \\ \cdot \\ \cdot \\ \cdot \\ f_{2n} \end{bmatrix} \qquad (2.8)$$

It is known that

$$f_{2i}(u,v) = \iint f_{1i}(x,y)e^{-j\left(\frac{2\pi xu}{\lambda_i f} + \frac{2\pi yv}{\lambda_i f}\right)} \, dxdy \qquad (2.9)$$

We assume that the focal distance f is constant for all $\lambda_i$.

The intensity of the field at any point with coordinates $(u,v)$ in the image plane is given by

$$\Phi(u,v) = F_2^{*T}(u,v)F_2(u,v) = \sum_{i=1}^{n} f_{2i}^{*}(u,v)f_{2i}(u,v) \qquad (2.10)$$

where the $*$ indicates conjugate. Cross terms such as $f_{2i}^{*}(u,v)f_{2j}(u,v)$ do not contribute to the intensity since their temporal frequency $w_i$ and $w_j$ are distinct. Let us now compute one component of Eq. (2.10) namely

$$\Phi_i(u,v) = f_{2i}^{*}(u,v)f_{2i}(u,v) \qquad (2.11)$$

Taking the Inverse Fourier transform $F^{-1}$ of both sides of Eq. (2.11) one obtains

$$F^{-1}\Phi_i(u,v) = f_{1i}(x,y) * f_{1i}^*(-x,-y) = \phi_i(\Delta_1,\Delta_2) \tag{2.12}$$

where the operator * means two-dimensional spatial convolution, and $\phi_i(\Delta_1,\Delta_2)$ is given by

$$\phi_i(\Delta_1,\Delta_2) = \iint f_{1i}(x+\Delta_1, y+\Delta_2) f_{1i}^*(x,y)\,dxdy \tag{2.13}$$

The latter is the two-dimensional spatial autocorrelation of the $i^{th}$ component of the input signal after the transparency.

Remark - In one dimension, the Fourier transform of the autocorrelation of a wave signal is its power density spectrum. In the two dimensional case the Fourier transform of $\phi_i(\Delta_1,\Delta_2)$ is the field intensity in the image plane. Now the total expression for Eq. (2.10) is

$$\Phi(u,v) = \sum_{i=1}^{n} \Phi_i(u,v) = \sum_{i=1}^{n} \iint \phi_i(\Delta_1,\Delta_2) e^{-j\frac{2\pi}{\lambda_{if}}(u\Delta_1+v\Delta_2)}\, d\Delta_1 d\Delta_2 \tag{2.14}$$

## 2.4 Continuous Temporal Spectrum

In Sections 2.2 and 2.3 we considered a general discrete field where by discrete we mean sum of several monochromatic frequencies. Now we generalize to the case where the input signals have continuous temporal spectra.

Let the spatial magnitude $A_i(x,y)$ in the object plane be the product of a spatial component and a frequency domain component.

$$A_i(x,y) = A(x,y)H(jw)\delta(w-w_i)$$

where $A(x,y)$ is constant for all monochromatic components, and $\delta(w)$ is the unit impulse. The phase $\beta_i(x,y)$ is not of concern to us, since essentially the intensity in the image plane is independent of phase shifts.

With the above assumption, Eq. ( 2.14) can be written as

$$\sum_{i=1}^{n} \iint \phi(\Delta_1, \Delta_2) e^{-j\frac{2\pi}{\lambda_i f}(u\Delta_1 + v\Delta_2)} H(jw) H^*(jw) \delta(w - w_i) d\Delta_1 d\Delta_2 \qquad (2.15)$$

where $\phi(\Delta_1, \Delta_2)$ is identical for all monochromatic components. Since

$$\frac{1}{\lambda_i} = \frac{f_i}{c} \qquad (2.16)$$

$$\frac{2\pi}{\lambda_i} = \frac{w_i}{c} \qquad (2.17)$$

Therefore Eq. ( 2.15) is equal to

$$\sum_{i=1}^{n} \iint \phi(\Delta_1, \Delta_2) e^{-j\frac{w_i}{cf}(u\Delta_1 + v\Delta_2)} |H(w)|^2 \delta(w - w_i) d\Delta_1 d\Delta_2 \qquad (2.18)$$

In Eq. ( 2.18) one can assume the spectrum is continuous over a range

$$\Omega_1 < w < \Omega_2 \qquad (2.19)$$

In this case Eq. ( 2.18) reduces to

$$\int_{\Omega_1}^{\Omega_2} dw \iint_{-\infty}^{+\infty} d\Delta_1 d\Delta_2 e^{-j\frac{w}{cf}(u\Delta_1 + v\Delta_2)} \theta_{HH}(w) \phi(\Delta_1, \Delta_2) \qquad (2.20)$$

or

$$\iint_{-\infty}^{+\infty} d\Delta_1 d\Delta_2 \, \phi(\Delta_1, \Delta_2) \int \theta_{HH}(w) e^{-j\frac{w}{cf}(u\Delta_1 + v\Delta_2)} dw \qquad (2.21)$$

Now the temporal power density spectrum of the signal

$$\theta_{HH}(w)$$

and the temporal autocorrelation of the signal

$$\theta_{hh}(\tau)$$

are related by

$$\theta_{hh}(\tau) = \int_{-\infty}^{+\infty} \theta_{HH}(w) e^{jw\tau} \frac{dw}{2\pi}$$

Thus

$$\int_{\Omega_1}^{\Omega_2} \theta_{HH}(w) e^{-j\frac{w}{cf}(u\Delta_1 + v\Delta_2)} dw = 2\pi\theta_{hh}\left(\frac{u\Delta_1 + v\Delta_2}{cf}\right) \qquad (2.22)$$

Substitution of Eq. (2.22) in Eq. (2.18) renders

$$\Phi(u,v) = 2\pi\iint \theta_{hh}\left[\frac{-(u\Delta_1 + v\Delta_2)}{cf}\right]\phi(\Delta_1, \Delta_2)\, d\Delta_1\, d\Delta_2 \qquad (2.23)$$

Equation (2.23) is the main transfer functional. It relates $\Phi(u,v)$ to $\theta_{hh}$ and $\phi(\Delta_1, \Delta_2)$.

Consider as a special case monochromatic light. Then

$$\theta_{HH}(w) = \delta(w - w_0)$$

So

$$\theta_{hh}(\tau) = e^{jw_0\tau}$$

and

$$\theta_{hh}\left(-\frac{u\Delta_1 + v\Delta_2}{cf}\right) = e^{-j\frac{w_0}{cf}(u\Delta_1 + v\Delta_2)}$$

then

$$\Phi(u,v) = 2\pi\int_{-\infty}^{+\infty}\iint \phi(\Delta_1, \Delta_2) e^{-j\frac{w_0}{cf}(u\Delta + v\Delta_2)} d\Delta_1\, d\Delta_2$$

or

$$\Phi(u,v) \longleftrightarrow \phi(\Delta_1, \Delta_2)$$

where $\longleftrightarrow$ indicates Fourier transform pairs. Thus the formula for $\Phi(u,v)$ is in agreement with the results generally given for the case of monochromatic incoherent light.

## 2.5 Example and Discussion

Consider a signal with a temporal Gaussian power density spectrum as given in Fig. 2-1

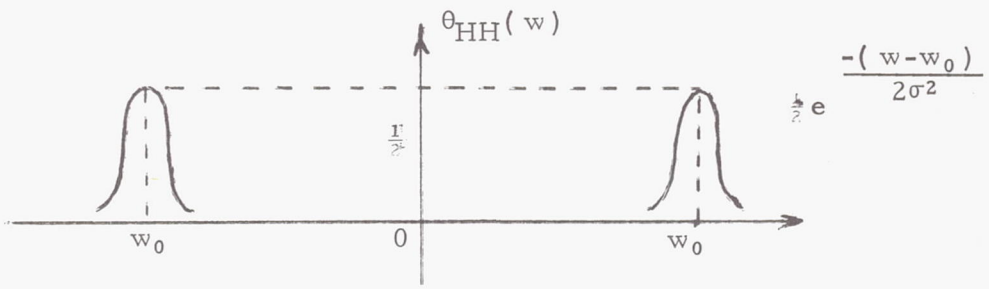


Fig. 2-1--Power Density Spectrum.

where $\sigma$ is fixed and is a measure of the coherence of the signal.

The inverse Fourier transform of $\theta_{HH}(w)$ can be easily obtained if we observe that $\theta_{HH}(w)$ is the convolution of two signals:

$$A(w) = e^{-\frac{w^2}{2\sigma^2}}$$

$$B(w) = \tfrac{1}{2}[\delta(w-w_0) + \delta(w+w_0)]$$

where $\delta(w)$ is the unit impulse. Thus if $a(t)$ and $b(t)$ are, respectively, the inverse Fourier transforms of $A(w)$ and $B(w)$

$$\theta_{hh}(\tau) = a(\tau)\, b(\tau)$$

For this example

$$b(\tau) = \cos w_0 \tau$$

$$a(\tau) = \frac{\sigma}{\sqrt{2\pi}} e^{-\frac{\sigma^2\tau^2}{2}}$$

$$\theta_{hh}(\tau) = \frac{\sigma}{\sqrt{2\pi}} e^{-\frac{\sigma^2\tau^2}{2}} \cos w_0 \tau$$

Now let the aperture of the system be circular with radius a, then

$$a(x,y) = 1 \qquad \text{if} \qquad r \leq a$$
$$a(x,y) = 0 \qquad \text{if} \qquad r > a$$

It follows that

$$\phi(\Delta_1, \Delta_2) = \begin{cases} a^2 \cos^{-1} \dfrac{\sqrt{\Delta_1^2+\Delta_2^2}}{2a} - \dfrac{\sqrt{\Delta_1^2+\Delta_2^2}}{2} \sqrt{1 - \dfrac{\Delta_1^2+\Delta_2^2}{4a^2}} & \text{if } \sqrt{\Delta_1^2+\Delta_2^2} < 2a \\ 0 & \text{if } \sqrt{\Delta_1^2+\Delta_2^2} > 2a \end{cases}$$

And also

$$\theta_{hh}\left(\frac{-u\Delta_1 - v\Delta_2}{cf}\right) = \frac{\sigma}{\sqrt{2\pi}} e^{-\frac{\sigma^2}{2}\left(\frac{u\Delta_1+v\Delta_2}{cf}\right)^2} \cos\frac{w_0(u\Delta_1+v\Delta_2)}{cf}$$

For this example the integral for the image intensity cannot be derived in closed form.

This example demonstrates that even for the simple case of circular aperture and Gaussian temporal power density spectrum the image plane intensity is difficult to compute exactly. This is one drawback of the transfer functional. Besides, one may have to compute this integral several times if the temporal power density spectra of the different stars in the field and the background power density spectrum are different from one another. However the transfer functional gives the density of the total signal in the image plane which can be computed once for the signal to be tracked and once for the interference intensity caused by background and other stars. Thus the transfer functional enables one to derive the image intensity as a sum of two signals $s_1(u,v)$ to be tracked and $s_2(u,v)$ the background intensity.

In addition, once the computer program necessary for computation of $\Phi(u,v)$ has been written, it can be used for any functions $\theta_{hh}(\tau)$, $\phi(\Delta_1, \Delta_2)$ and the effect of wedges, masks and reticles or any other transparency can be incorporated because it directly effects $\phi(\Delta_1, \Delta_2)$ and consequently the image intensity.

# III. PARAMETER ESTIMATION BY CROSS-CORRELATION

## 3.1 Introduction

The problem of finding the location of the star image with respect to some coordinate system and the amount of rotation of this image fall within the class of parameter estimation problems. This is essentially a two-dimensional problem analogous to the one-dimensional case where the arrival time of a signal whose wave form is exactly known is to be found. This is done by performing measurements on a received wave form that contains the signal of interest, and unwanted disturbance--noise and other deterministic signals.

In this part cross-correlation techniques that are easy to implement are discussed.

## 3.2 Cross-Correlation Technique

A natural tool in the implementation of pattern alignment is the cross-correlation function. In communication theory the one dimensional autocorrelation function of a deterministic function $f(t)$ is defined as

$$\phi(\tau) = \int_t f(t) f(t+\tau)\, dt$$

The autocorrelation is maximum for $\tau=0$. Thus if $f(t+a)$ is the received signal where a is unknown, one cross-correlates $f(t)$ with locally generated replicas of $f(t)$ with different parameters $f(t+\tau_i)$:

$$\phi(\tau) = \int_t f(t+a) f(t+\tau_i)\, dt$$

If

$$\phi(\tau_j) = \max_i \phi(\tau_i)$$

then

$$a = \tau_j$$

As an alternative scheme one could generate $\dot{f}(t+\tau_i) = \frac{df}{dt}(t+\tau_i)$ and form the cross-correlation

$$\dot{\phi}(\tau_i) = \int f(t+a)\,\dot{f}(t+\tau_i)\,dt$$

Then the search would be for that particular value of $\tau_j$ that makes

$$\dot{\phi}(\tau_i) = 0$$

which is

$$\tau_j = a$$

These ideas can be extended to the two dimensional case for aligning spatial patterns. The image of a star pattern can be represented as a two dimensional spatial signal. Suppose that when this image is properly aligned on some plane in the star-tracker system the light intensity across the plane is given by $f(x,y)$. Then if the pattern is misaligned the intensity distribution will be $f((x+k)\cos\theta - (y+h)\sin\theta, (x+k)\sin\theta + (y+h)\sin\theta)$. That is to say, the distribution would be correct if it were rotated through an angle $-\theta$ and shifted forward along the x and y axes by amounts k and h, respectively. The autocorrelation can now be defined as

$$\phi(k,h,\theta) = \iint_{x\,y} f(x,y)\,f((x+k)\cos\theta-(y+h)\sin\theta, (x+k)\sin\theta+(y+h)\cos\theta)\,dy\,dx$$

This will be maximized for $k = h = \theta = 0$. The autocorrelation and related functions can be measured in several ways, some optical and some electronic. One optical technique which can be used with incoherent light is to make a positive photographic transparency of $f(x,y)$ and focus the shifted image on this transparency. A condenser lens can be used as shown in Fig. 3-1 to focus the resulting light on a small area of a photomultiplier tube whose output, being the two dimensional spatial integral of the light falling on it, is the desired cross-dorrelation. This method has the disadvantage that the value of $\phi(k,h,\theta)$ does not necessarily uniquely define k, h and $\theta$ so that knowing $\phi(k,h,\theta)$ does not necessarily help in aligning the image properly. It only indicates that the image is or is not properly aligned. A related method[1] can be used to systematically correct for h, k and $\theta$.

Besides even if unique values for k, h and $\theta$ would result from computation, the problem is essentially a three dimensional search for the maximum of $\phi$. This itself is a difficult problem. Also more accuracy would require higher resolution which in turn would require small search steps and consequently more measurements or processing.

## 3.3 Prefiltering

Up to now most investigators using optical correlation techniques for star-tracking have used $\phi(k, h, \theta)$ that results from correlating a star field image with the stored replica of itself. If the cross-correlation processing is done by digital means, the system can scan the input image with a vidicon or by some other means and cross-correlate an encoded version of this image with a reference function stored in digital form. Many systems which process the image signals electronically have been devised, some using cross-correlation techniques and some not. However these systems all seem to have one important aspect in common with systems where optical cross-correlation is performed: namely, the optical image is almost always accepted in its simplest form with little or no thought given to the possibility of preprocessing this image in some way that will improve the performance of the system.

It would be advantageous to change $\phi(k, h, \theta)$ by prefiltering in order to facilitate its manipulation and processing. The following heuristic discussion is pertinent to such a prefiltering.

A heuristic discussion is preferable at this time because the mathematical development of Part II, although very useful for analysis, does not lend itself to synthesis very easily. The difficulties that would be encountered in synthesis of the desired filter in the focus of the objective length are threefold:

1. From the desired autocorrelation function, the desired image intensity distribution must be found. This requires solution of a nonlinear integral equation.

2. Knowing the desired image intensity and temporal power density spectrum of the source, one can use Eq. (2.23) to find the desirable spatial autocorrelation $\phi(\Delta_1, \Delta_2)$ at the focus of the objective lens. This is a linear integral equation.

3. Finally, one must use $\phi(\Delta_1, \Delta_2)$ to derive the desired filter. This step again requires solution of a nonlinear integral equation.

Suppose that a star field image intensity is described by $f(x,y)$ whose autocorrelation is $\phi_f(k,h,\theta)$. If an appropriate spatial filter is introduced in the system, a new intensity function $g(x,y)$ will result. Its autocorrelation, $\phi_g(k,h,\theta)$, will be different from $\phi_f(k,h,\theta)$ and may be better suited to the purpose of parameter estimation.

To clarify this, consider the system shown in Fig. 3-1, which measures $\phi(k,h,\theta)$ by the method described above. The system consists of an objective lens, a reference transparency, a condenser lens and a photomultiplier tube whose output is $\phi(k,h,\theta)$.

For simplicity suppose there is only one star in the field. The reference transparency is a picture of the image of that star. Roughly speaking, $f(x,y)$ is zero except inside a small circle and so $\phi_f$ is zero except when the image is almost perfectly aligned with the reference. This means that a knowledge of $\phi_f$ is not particularly helpful in lining up the image unless near perfect alignment has already been achieved. Until this state has been reached no information is present which makes movement in one direction any more logical than movement in another. Even when the stage where the cross-correlation is no longer zero is reached, gradient techniques must be resorted to and these can be very time consuming.

Suppose an appropriate filter is inserted at point A (Fig. 3-1) so that the image intensity, instead of being a circle has the form of a cross. Consequently, the reference transparency inserted at point B (Fig. 3-1), namely $g(x,y)$ must be also in the form of a cross. The cross-correlation of the reference transparency and the star image reduces to cross-correlation of two cross (Fig. 3-2). Now the image can be aligned quite easily. First it is moved back and forth in the x-direction until a cross-correlation peak is found. The alignment of Fig. 3-3a will result.

Then the image is moved back and forth in the y-direction with the result that the absolute maximum of the cross-correlation is achieved and the image is properly aligned as shown in Fig. 3-3b.

This illustration shows that the form of $\phi$ has an extremely important bearing on the practicality of a star tracker that uses cross-correlation, and that one class of image intensities that provide reasonably simple processing is the cross type.

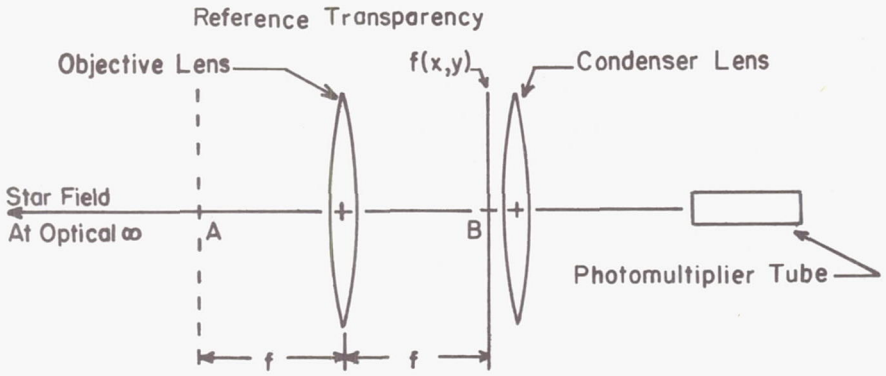


Fig. 3-1. Optical Cross-correlator.

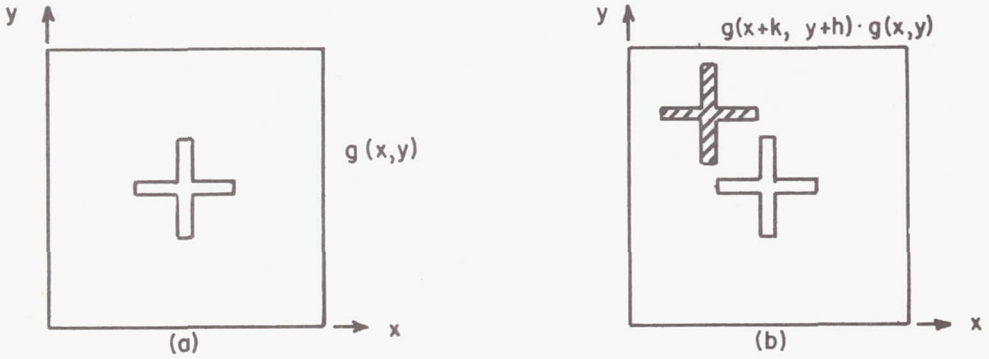


Fig. 3-2. (a) Reference Transparence. (b) Reference Transparency and Superimposed Star Image.

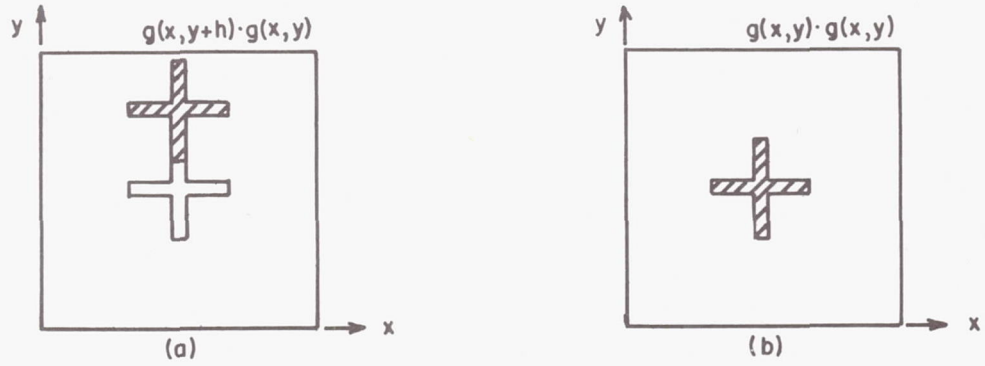


Fig. 3-3. (a) Result of Search in x-direction. (b) Result of Search in y-direction.

A primary consideration in such a system is of course the accurate determination of the exact location of the center of each star image. In the past, considerable attention has been given to prefiltering in order to concentrate the energy of each star image in the smallest possible area in the image plane. This would reduce the uncertainty in the location of its center. However, as was well known to the people studying this problem, very little can actually be done along this line since a principle analogous to the uncertainty principle in quantum mechanics operates here. Simply stated, this principle says that the product of the system's optical aperture and the width of its spread function* is always greater than some constant. This means that without increasing the optical aperture, the image of a star cannot be made smaller once a certain size has been reached.

Thus at first sight it would appear that prefiltering of the image does not offer much help. Yet this is not necessarily the case. As an example, consider a system which scans the image with a vidicon tube to translate it into electrical signals. This system divides the image up into an array of small cells each one having a certain intensity and representing a sample of the image. The dimension of each cell is, in one direction, a function of the electron beam spot size and, in the other direction, a function of the band width of the vidicon's output signal. All the information about the x and y coordinates of a star is contained in a very small number of cells. It is clear that with certain types of noise this system will be vulnerable to serious errors.

So it would seem that for this type of system preprocessing which concentrates the star's image in a smaller area could actually be detrimental. It might be better to actually spread the energy out so that it covers many cells and then average over these cells to reduce the error due to noise. The star cross pattern mentioned earlier does exactly this. It spreads out the energy along the x and y axes so that a great many samples of both the x and y coordinates are available. By averaging over these samples it should, for certain types of noise, be possible to reduce the size of the error.

### 3.4 Conclusion

It has been argued that certain types of prefiltering of the optical signal are desirable in order for the image intensity to have a definite form. This definite form--shape of a cross--has strong gradients in two orthogonal directions and thus would render simple implementation of cross-correlation techniques. In addition, it appears that the prefiltering method proposed here has advantages for certain types of sensor noise and digital processing.

---

* The spread function is the image of a point source. Since stars are nearly point sources their images are approximately the same as the spread function.

# IV. EXPERIMENTAL RESULTS

## 4.1 Introduction

In Part III it was shown that it would be desirable to fabricate an amplitude filter which would be placed in front or immediately behind the objective lens of the star-tracking system. The filter would be such that each star in the field of view would appear as a cross-type diffraction pattern in the image plane of the objective lens. If for example there were three stars in the field of view, there would be three cross-type diffraction patterns in the focal plane of the objective lens. If the photoconductive surface of a vidicon pick-up tube were aligned with the image plane of the objective lens, each cross-type diffraction pattern could be sensed.

The basic idea behind all of the experimental results reported in this part was to provide some general guidelines which may be used to design an amplitude filter which will diffract as much of the incident energy as possible into the diffraction tails which form a cross-type diffraction pattern. Although each of the experiments were performed with a particular light intensity and aperture size, the conclusions were general enough to be applicable to systems with other parameters--including systems using a Cassegrainian telescope.

In Section 4.2 the simulation of the star field and characteristics of the apparatus used will be discussed. In Section 4.3 the experiments and results are presented chronologically. Finally, the conclusions are presented in Section 4.4.

## 4.2 Simulation

A single star on the optical axis was simulated by both monochromatic light from a Spectra-Physics, Model 115, three milliwatt laser with a 6328 $A^{\circ}$ (red) wavelength and a 100 watt relatively broad-band mercury-arc lamp. With either source the next step was to insert a diverger lens, pinhole and collimator lens between the light source and the filter. The extremely small pinhole (2 micron diameter) was

assumed to simulate a star and the collimator lens was assumed to make the star appear to be an infinite distance away from the filter and the objective lens. The simulation system is shown in Fig. 4 -1.

The pinhole and light source for all of the experiments reported in this part were located in the optical axis. The intersection point of the two diffraction tails of the cross-type diffraction pattern was at the center of the incident energy from the simulated star. However, even if a star were not aligned with the optical axis, the point of intersection of the two diffraction tails would still be at the center of the diffraction pattern--provided that the objective lens were properly corrected for astigmatism and distortion.

All of the experiments reported in this part were performed with the filter--an amplitude transmission grating--positioned between the collimator and the objective lens. More will be said about this filter later. In this simulation the vidicon was replaced by an Exa camera with a 1/250 second exposure time. The regular Exa camera lens was removed, however, to permit use of the 350 mm lens as the objective. This longer focal length resulted in a large and clear image in the film plane of the camera. The film plane of the camera was positioned so that it coincided with the focal plane of the objective lens by ( 1) placing a ground glass screen in the focal plane of the camera and using a telescope mounted on the bench to view the image formed on the ground glass screen and align the distance between the camera and objective lens and ( 2) taping a mirror on the front surface of the ground glass screen to make sure that the beam reflected from the focal plane of the camera coincided with the incident beam. In this manner the entire film plane was brought into sharp focus.

Several comments are necessary here to relate this simulator to an actual star tracker. In an actual star-tracking system some space could be saved by placing the filter immediately after the objective lens. When an amplitude filter is used in front of the objective lens the distance between the filter and the objective lens has little or no effect upon the observed results. However, if space were saved by placing the filter after the objective lens, the size of the diffraction pattern would be affected by the distance between the filter and the objective. The closer the filter is positioned to the objective, the larger the diffraction pattern in the focal plane.

It is important that the objective lens be corrected for chromatic aberration so that the incident broadband energy can be brought to a focus in one plane. The need for a mechanical sun-shutter could be eliminated if the glass in the objective lens and/or vidicon window were

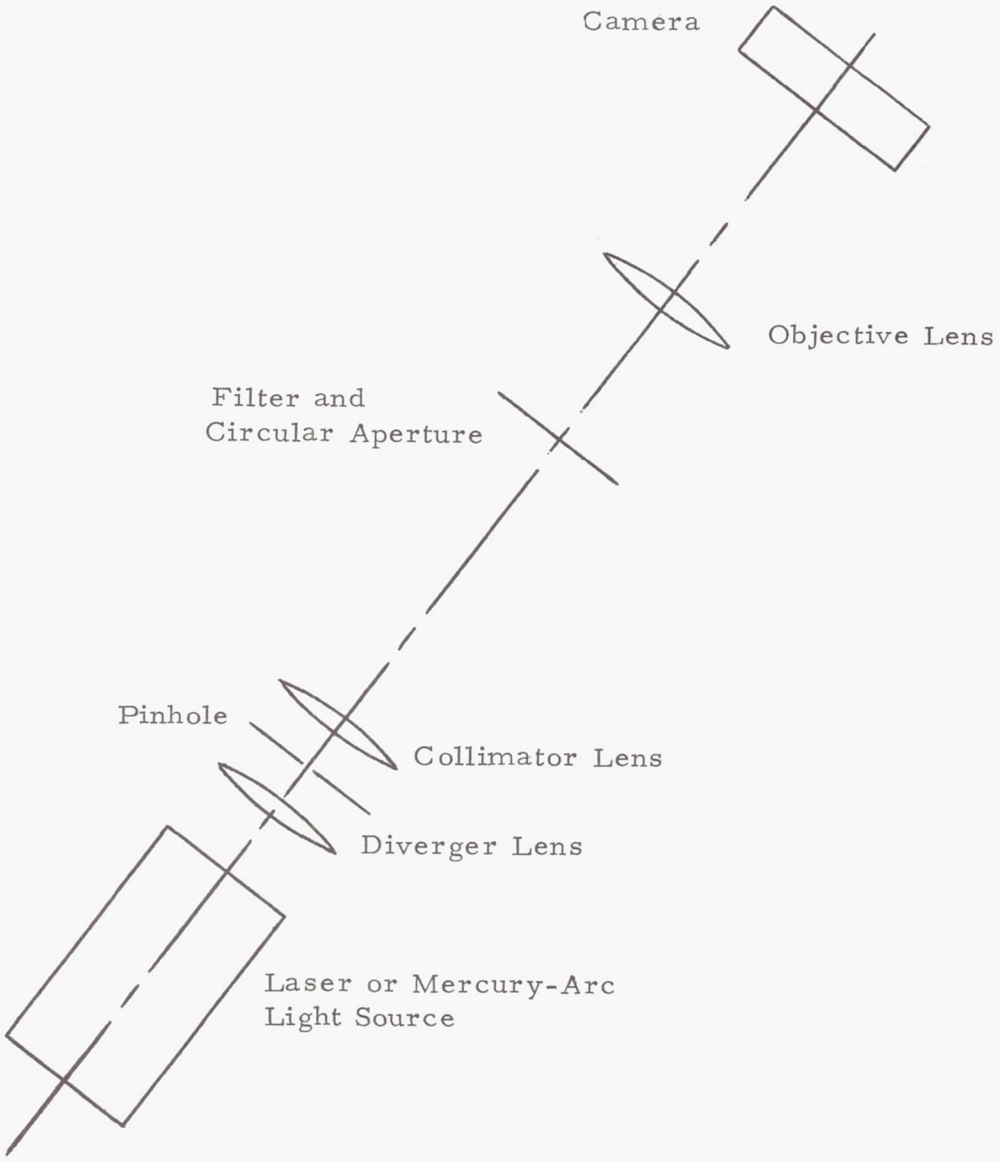


Fig. 4-1--The Simulation System

fabricated out of encapsulated photochromic material that turned opaque when irradiated with very intense energy. The glass in the objective lens and/or vidicon window should pass only that part of the energy spectrum to which the photoconductive surface of the vidicon is sensitive. Any additional energy would only be transformed into heat at the photoconductive surface and increase system nonlinearities.

## 4.3 Experiments and Results

In the following experiments the variables were first identified and manipulated by performing experiments with the monochromatic laser light source. Then, the broadband mercury-arc light source was used to determine the effect of using a source with a more star-like broadband spectrum. The mercury-arc source specifications showed six narrow emission bands ranging from red to ultraviolet. Four of the bands--red, yellow, green and blue--were clearly visible when viewed through a non-achromatic objective lens. For this reason a Topcor achromatic lens was used to photograph all of the mercury-arc diffraction patterns. The 50mm Topcor brought all of the light to a focus at the film plane of the camera. However, the image was not nearly as large as that which was obtained with laser diffraction patterns because a non-achromatic 350mm objective lens could be used with the monochromatic light source. The mercury-arc pictures in this chapter did not show as much detail and had to be enlarged about three times more than the laser pictures.

In all of the laser pictures, the central portion of the cross-type diffraction patterns have been overexposed to facilitate easier observation of effects of interest in the diffraction tails. At the end of this part, some mercury-arc photographs are shown which were taken at a reduced intensity to make the resulting diffraction pattern comparable with a pattern which was visually observed while viewing the star Vega with binoculars and using a 3-mesh ( three wires/inch) wire screen as an amplitude transmission filter.

Figure 4-2a will be used to ( 1) provide a starting point for subsequent experimentation and ( 2) show a correlation between these results and the theoretical discussion of diffraction theory by Born and Wolfe.[2]

Figure 4-2a shows the diffraction pattern obtained with an 18-mesh wire screen used as a filter. The filter is shown in Fig. 4-2b and consists of the wire screen with a 0.542 inch circular aperture which served only to control the amount of incident radiation by reducing the effective diameter of the objective lens. Except where noted the 0.542 inch circular aperture

Fig. 4-2-Laser

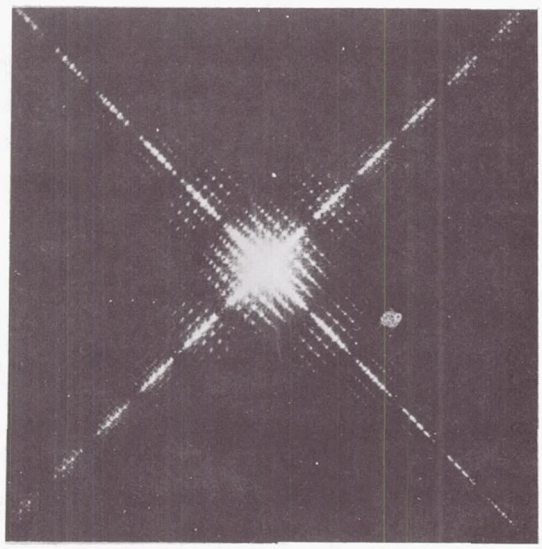

(a)

(b)

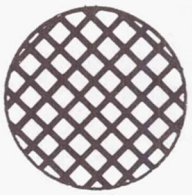

Fig. 4-3-Laser

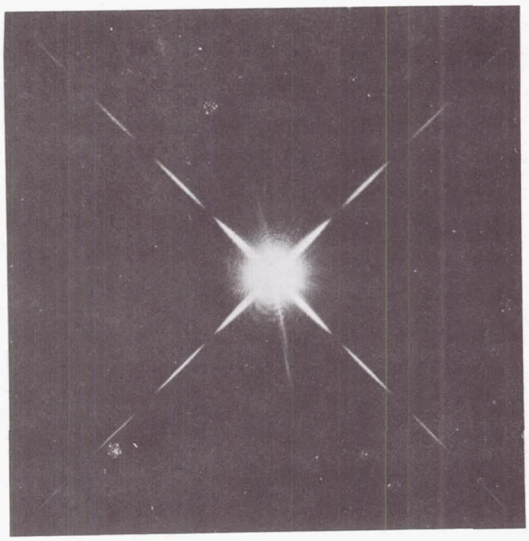

(a)

(b)

Fig. 4-4 Laser

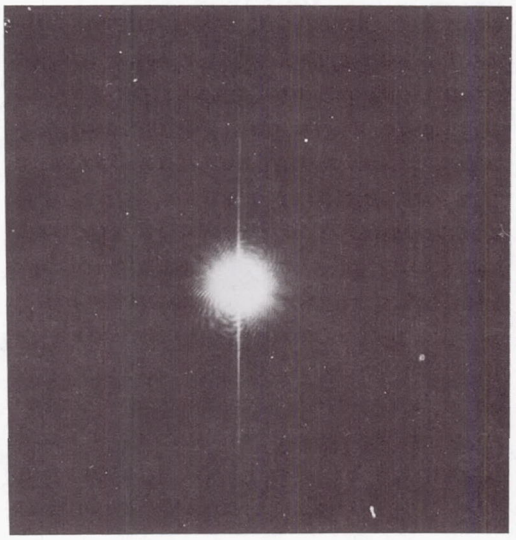

(a)

(b)

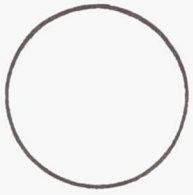

was used with all of the filters discussed in this report.

The wires of the filter extending from the lower-left to upper-right of Fig. 4-2b caused the dashed diffraction-tail which extends from upper-left to lower-right in Fig. 4-2a. The wires from upper-left to lower-right in Fig. 4-2b gave rise to the dashed diffraction tail which extends from lower-left to upper-right in Fig. 4-2a.

The dots which form a square array near the overexposed center section and extend outward from the dashes in the diffraction tails were present whenever there were more than two parallel wires in the filter. The presence of these dots will be referred to as a spreading effect. In Fig. 4-2a there is a considerable amount of spreading whereas in Fig. 4-3a there is no spreading. Figure 4-3a was made under identical conditions except the filter consisted of only two perpendicular wires. For the purposes of star-tracking, it will be assumed that spreading is an undesirable effect and therefore something to be reduced or eliminated.

The vertical line which crosses through the overexposed center section of both figures was an artifact which was caused by the shutter movement in the Exa camera. The Exa shutter was horizontal and moved up and down when the picture was taken. This caused the vertical artifact even though the shutter was located only one-sixteenth inch away from the film plane. In an actual star-tracking system of this nature there would be no shutter and hence no shutter artifact. The filters were always placed so that the shutter artifact would not overlap with the diffraction tails.

The shutter artifact in Fig. 4-2a is considerably fainter than in Fig. 4-3a. This provides an indication that the intensity of the irradiant energy at the overexposed intersection point was less for the 18-mesh, 16 wire filter in Fig. 4-2 than it was for the 1-mesh, 2 wire filter in Fig. 4-3. It may be inferred that a higher percentage of the incident energy was diffracted by the 18-mesh filter shown in Fig. 4-2b. A control picture with no wire filter and only the 0.542 inch circular aperture is shown in Fig. 4-4a. Here the shutter artifact was even more intense, as would be expected since there was no filter and all of the incident energy was concentrated in the central area.

The intensity of the diffraction pattern shown in Fig. 4-2a can be described by the equation

$$I(p,q) = C\left(\frac{\sin\frac{Nkdp}{2}}{\sin\frac{kdp}{2}}\right)^2\left(\frac{\sin\frac{ksp}{2}}{\frac{ksp}{2}}\right)^2\left(\frac{\sin\frac{Nkdq}{2}}{\sin\frac{kdq}{2}}\right)^2\left(\frac{\sin\frac{ksq}{2}}{\frac{ksq}{2}}\right)^2 \qquad (4.1)$$

where

$I(p,q)$ = intensity at point $(p,q)$ where p and q are as shown in Fig. 4-2a.

N = A constant approximately equal to the number of open spaces between parallel wires in the filter ( $N \simeq 9$ ).

$k = \frac{2\pi}{\lambda}$

d = The distance ( center-to-center ) between wires.

s = The width of the opening between parallel wires.

C = A constant which is proportional to $s^4$ and the diameter of the aperture and inversely proportional to the wavelength ( $\lambda$ ) of the laser ( 6328 $A^\circ$ ).

The term $\left(\frac{\sin\frac{Nkdp}{2}}{\sin\frac{kdp}{2}}\right)^2$ has principal maxima whenever $\frac{kdp}{2}$ is some multiple of $\pi$. Since $k = \frac{2\pi}{\lambda}$, these maxima occur every $\frac{\lambda}{d}$ units on the p axis. Inspection of Fig. 4-2a shows that each dash ( on a diffraction tail) actually is not a dash at all but consists of four principal maxima. These maxima are separated by $\frac{\lambda}{d}$ units on the p or q axis. All of the dots in the areas where spreading occurs are also separated by $\frac{\lambda}{d}$ units. In addition there are N-2 submaxima between each principal maxima. Many of these submaxima were visible when the film was observed under a microscope.

The $\left(\frac{\sin\frac{ksp}{2}}{\frac{ksp}{2}}\right)^2$ term has a null whenever $\frac{ksp}{2}$ is a multiple of $\pi$.

It may be observed from Fig. 4-2a that the first null occurs at a distance of $5 \times \frac{\lambda}{d}$ on the p axis. This does not necessarily mean that the first null of $\sin\frac{ksp}{2}$ occurs at a distance of $5 \times \frac{\lambda}{d}$ on the p axis. It does mean that some null of $\sin\frac{ksp}{2}$ occurs at a distance of $5 \times \frac{\lambda}{d}$ on the p axis.

For 18-mesh wire screen with each wire having a diameter of 0.011 inch

$$d = \frac{1.000}{18} = 0.0556 \qquad (4.2)$$

and

$$s = d - .011 = 0.04456 \text{ inch.} \qquad (4.3)$$

Hence,

$$s \approx 4/5\, d. \qquad (4.4)$$

So the fourth null of $\left(\frac{\sin\frac{ksp}{2}}{\frac{ksp}{2}}\right)^2$ occurs at the same point on the p axis as the fifth principal maximum of $\left(\frac{\sin\frac{Nkdp}{2}}{\sin\frac{kdp}{2}}\right)^2$. This explains why the fifth principal maximum is missing. From Eq. (4.3) it would be expected that the eighth and twelfth nulls of $\left(\frac{\sin\frac{ksp}{2}}{\frac{ksp}{2}}\right)$ would cancel out the tenth and fifteenth principal maxima of $\left(\frac{\sin\frac{Nkdp}{2}}{\sin\frac{kdp}{2}}\right)^2$ and inspection of Fig. 4-2a verifies that this was the case. If the central portion were not overexposed the width of the intersection point would be about $2 \times \frac{\lambda}{d}$.

Inspection of Eqs. (4.2) and (4.3) reveals that the relationship between s and d in Eq. (4.4) was highly dependent upon the diameter of the wire. In fact the distance to a specific null is inversely proportional to the wire diameter. The wire diameter of the two wire filter in Fig. 4-3b was .007 inch. Figures 4-5a and 4-6a show diffraction pattern obtained from single wire filters with wire diameters of .00443 inch and .00663 inch, respectively. These diameters were chosen so that their ratio was about 1.5. Using the two wires together, the second maxima of the large wire cancelled the first null of the small wire and the first and second maxima of the small wire cancelled the first and second nulls of the large wire. This apodization effect is shown in Fig. 4-7a-d for various separations of the two wires. The best apodization occurred when the two wires were separated by a distance about equal to the radius

Fig. 4-5--Laser

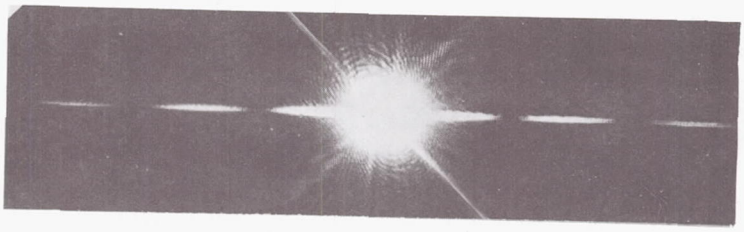

(a) (b)

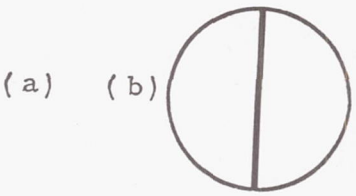

Fig. 4-6--Laser

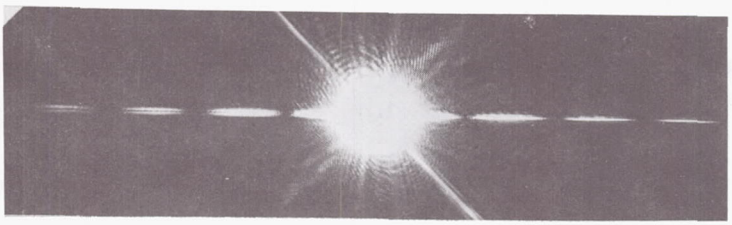

(a) (b)

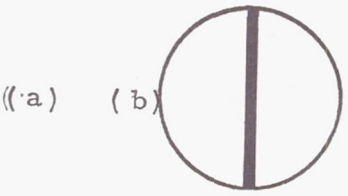

Fig. 4-7--Laser

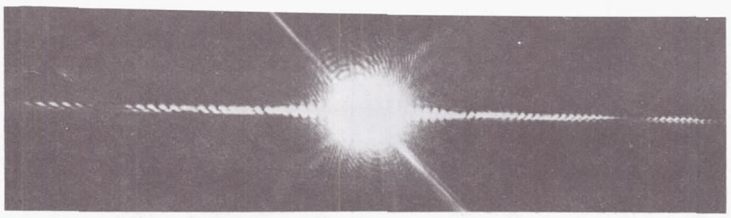

(a)

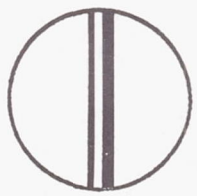

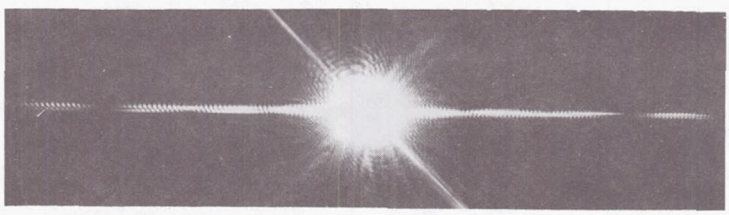

(b)

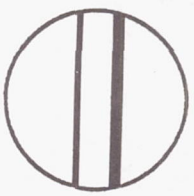

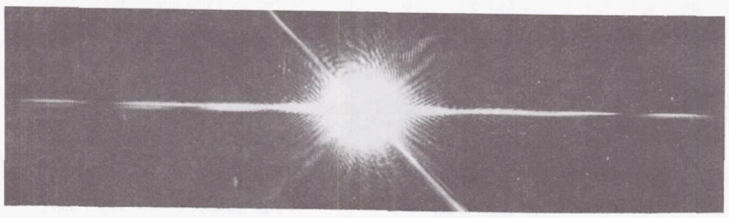

(c)

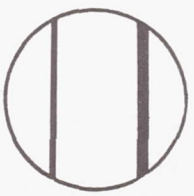

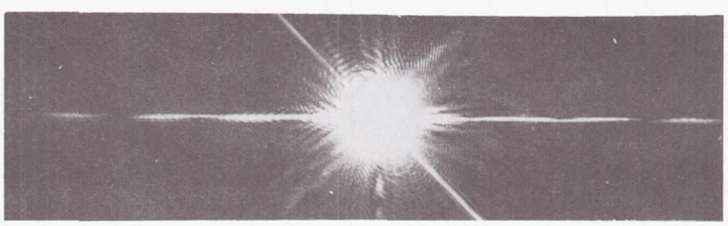

(d)

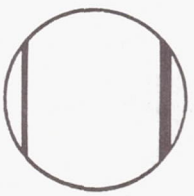

of the 0.542 inch circular aperture. This case is shown in Fig. 4-7c. The next null could be removed by using a third wire of appropriate diameter.

Since the incident energy from a star field is small, it is absolutely necessary to diffract as much of this energy as possible into the diffraction tails to facilitate sampling by a vidicon in a real system. Analysis of the shutter artifact intensity of Figs. 4-2, 3 and 4 suggests that both the intensity of diffracted energy and the amount of spreading decreased as the number of wires in the filter was decreased from 16 to 2. Since spreading is undesirable, it was postulated that some optimum number of wires exists for which the amount of diffracted energy is high while the spreading is low.

Figure 4-8a-c shows that the spreading effect was dependent upon the total number of wires in the filter. The amount of spreading was about equal in both diffraction tails whenever there were eight wires in one direction and only two wires in the other direction ( Fig. 4-8c).

Figure 4-9 confirms that three parallel wires cause more energy to be diffracted than a single wire. It should be recalled that the diffraction tail from lower-left to upper-right is caused by the filter wires extending from upper-left to lower-right and vice-versa. The contrast becomes quite apparent when the intensities of the fifth or sixth dash are compared.

Since the spreading effect depends upon the total number of wires in the filter and it was desirable to maintain equal intensities in both of the diffraction tails, the optimum filter would have an equal number of wires in both directions. Figure 4-10a-c shows how many wires it was necessary to remove to significantly reduce the spreading effect. A similar trade off would exist in systems with other aperture sizes and parameters.

Figure 4-11 shows some photographs that were taken while using the broadband mercury-arc source. The exposure time and light level were controlled so that the results could be compared with visual observations of the star Vega with binoculars and a 3-mesh wire filter. Figure 4-11a is a control picture taken with no prefilter other than the circular aperture. Figure 4-11b shows that the dashes in the diffraction tails were still present with a broadband light source and that the distance to a specific null was still inversely related to the wire diameter. Figure 4-11c shows the effect of adding six more wires and apodization. The nulls are less apparent than in Fig. 4-11b. The visual observation of Vega was more similar to Fig. 4-11b in terms of the apparent per

Fig. 4-8-Laser

(a) (b) (c)

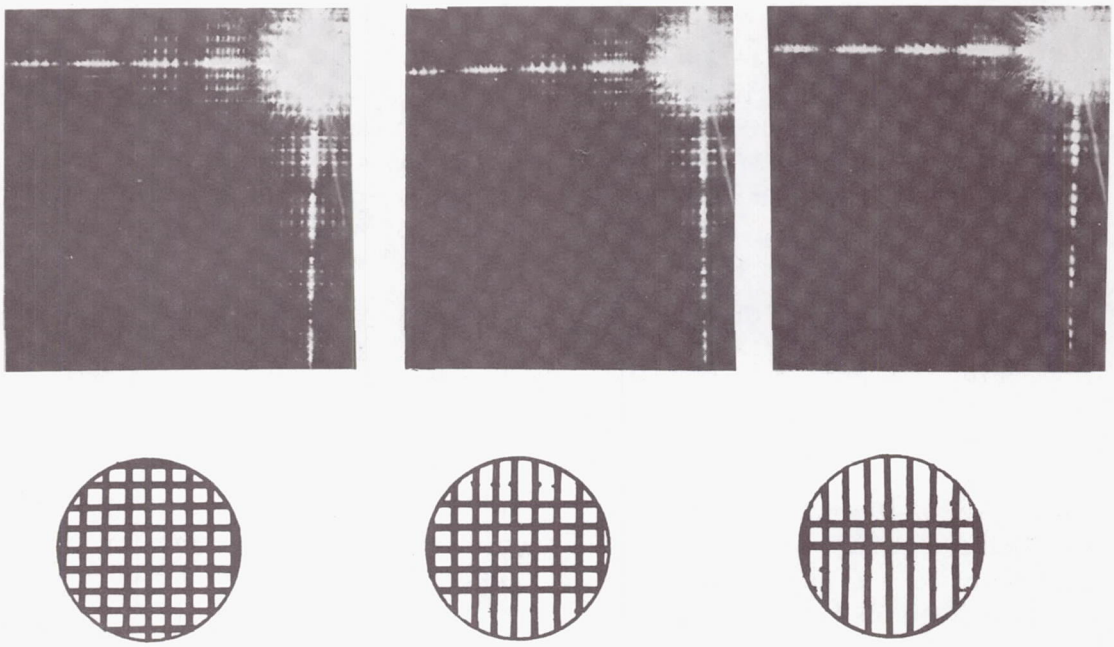

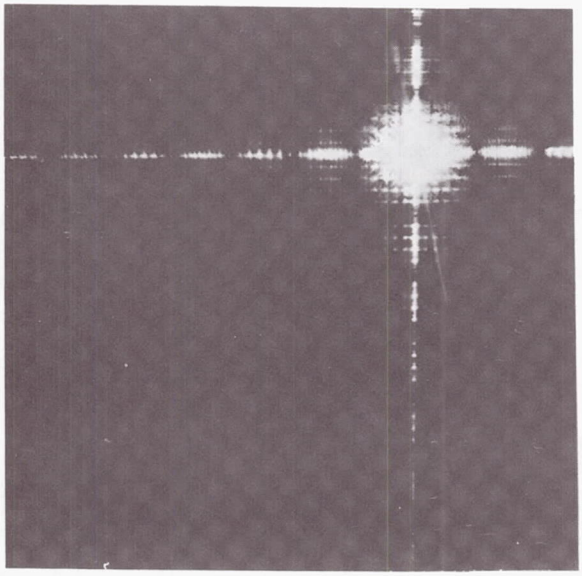

Fig. 4-9-Laser

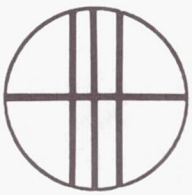

Fig. 4-10-Laser

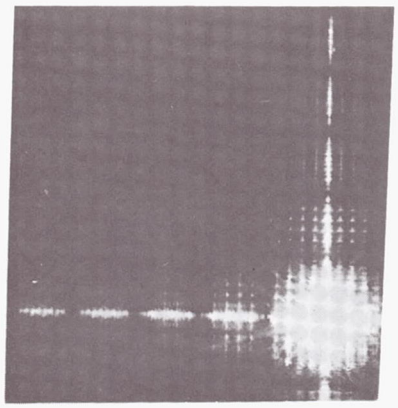

(a)

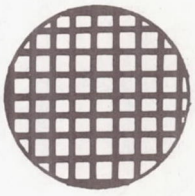

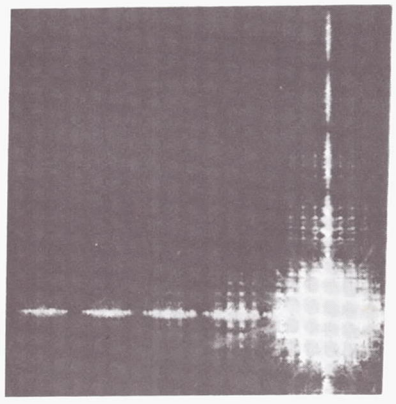

(b)

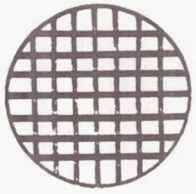

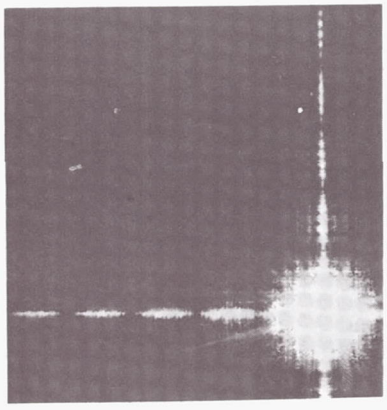

(c)

Fig. 4-11--Mercury-Arc

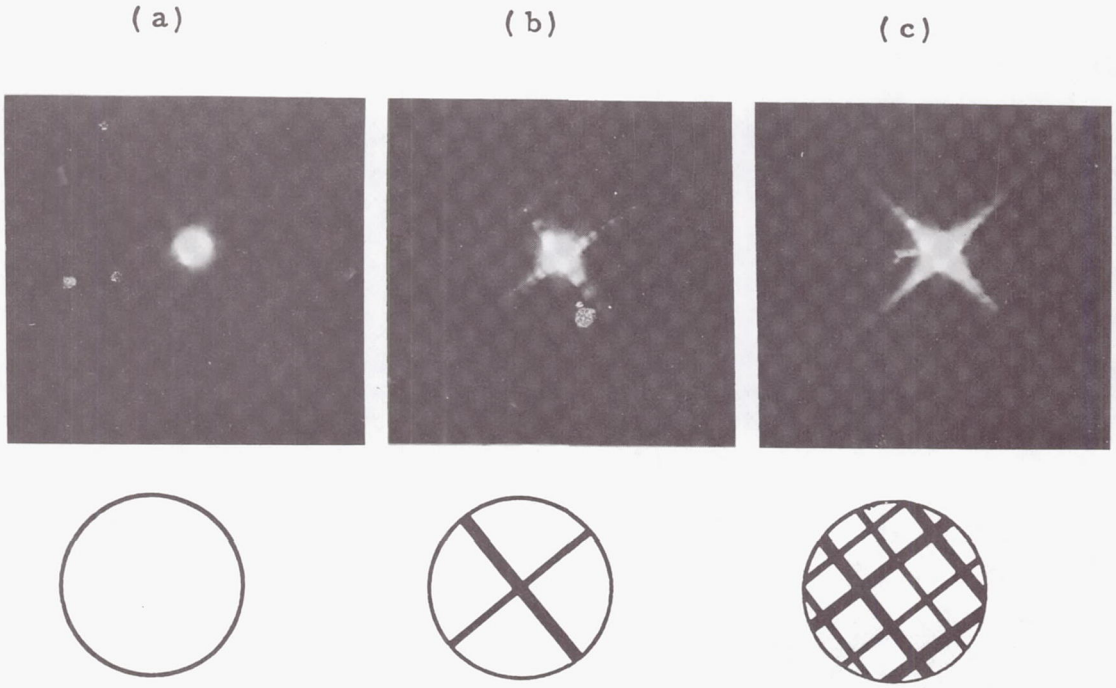


Fig. 4-12--Mercury-Arc

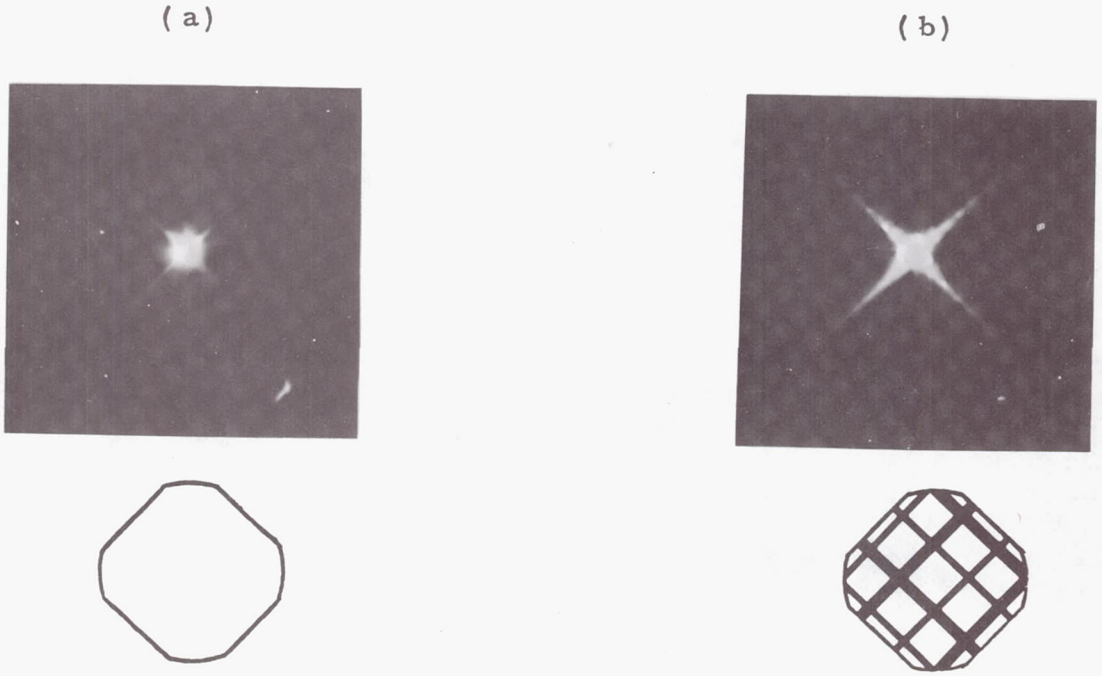

cent of energy which was diffracted away from the central portion of the diffraction pattern and the presence of nulls. The null areas in the diffraction tails were longer than those shown in Fig. 4-11b. This was due in part to the longer focal length of the binocular objective lens. However, it appeared that efficient apodization techniques would be even more necessary and useful in a real system than the simulation results tend to show. The spreading effect does not show up as dots in either the mercury-arc broadband simulation or the visual observation of Vega with a 3-mesh screen, although some widening of the diffraction tails does occur. Observation of Vega with an 18-mesh filter did produce a spreading effect with dots similar to Fig. 4-2.

The effect of using a noncircular aperture is shown in Fig. 4-12. These photographs may be directly compared with those of Fig. 4-11. The reason that a circular aperture has been used in all of the previous filters was because the lens will always be circular. Any filter which permits the irradiant energy from a star to enter all portions of the lens has in effect a circular aperture with a diameter equal to the diameter of the lens. The area of the filter shown in Fig. 4-12a was less than the area of the circular aperture because such a filter would not permit irradiant energy from a star to be incident upon all portions of the lens. The resulting diffraction pattern appears to have somewhat less spreading than that obrained with a completely circular aperture.

## 4.4. Conclusions

1. A spreading effect resulted when too many wires were used in the filter. The spreading effect was equal in both diffraction tails and depends upon the total number of wires in the filter.

2. The distance to a given null was inversely proportional to the wire diameter.

3. Apodization or removal of some nulls was achieved by using wires with different diameters.

# V. FURTHER EXPERIMENTAL RESULTS

## 5.1 Introduction

This part of the report is a continuation of the simulation work started in Part IV. The quality of the simulated star obtained with the mercury-arc light source was improved upon and some results are shown in Section 5.2. Section 5.3 describes a way in which the cross-type diffraction pattern might be utilized to develop a one-lens sun tracker capable of providing separate X and Y error signals. Some cross-correlation results are explained in Section 5.4 and general conclusions for Parts IV and V are presented in Section 5.5.

In general the 100W Osram (HBO 100W/2 No. 3110ka) mercury-arc source provides a superior simulation of the star than the helium-neon laser because the spectral distribution is more similar to most stars than the monochromatic laser. The reasons for using the laser more often than the mercury-arc source were because (1) in some cases it was easier to pass judgement on the results of manipulation of one parameter at a time, and (2) the best lenses available for use in the laboratory were specially designed for use with the monochromatic laser.

## 5.2 Some Improved Mercury-Arc Photographs

In all of the mercury-arc and laser photographs in this report a Perkin-Elmer Collimator Lens Assembly was used to provide a star-like point source. This assembly included the diverger lens, pinhole, and collimater lens shown in Fig. 4-1. Adjustments are provided to move the pinhole up and down with respect to the optical axis and in and out with respect to the diverger lens. It was determined that when switching from the laser to the mercury-arc source more uniform and spatially coherent simulated stellar radiation could be obtained by moving the pinhole closer to the diverger lens.

This adjustment facilitated the improved mercury-arc photographs shown in Fig. 5-1. The beneficial apodization effect may be observed in Fig. 5-1a. This effect resulted from the use of wires with different diameters in the filter. Some faint undesirable spreading

Fig. 5-1--Mercury-Arc

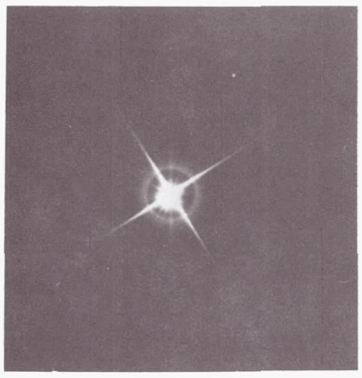

( a )

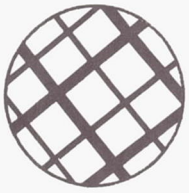

Fig. 5-2--Sun

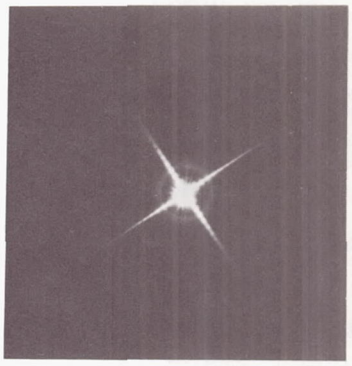

( b )

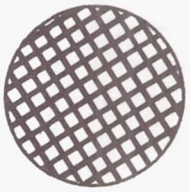

Fig. 5-3--Sun Tracker Image Dissector Camera Tube Apertures with Superimposed Cross Diffraction Pattern.

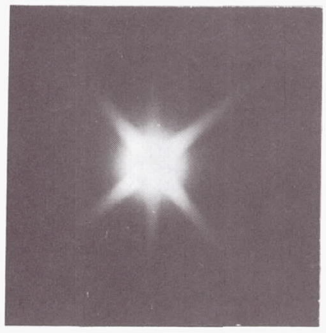

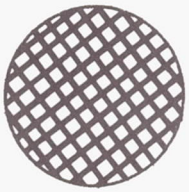

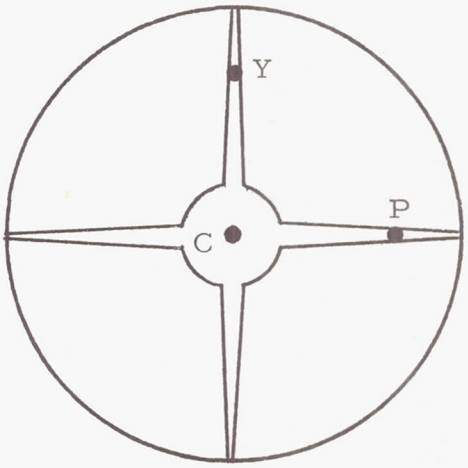

effects resulting from the use of too many wires in the filter is shown in Fig. 5-1b.

## 5.3 Feasibility of Sun Tracker Application for the Cross-Type Diffraction Pattern

Figure 5-2 shows a photograph of the noon sun made with a 35mm Exa Camera (f4, 1/250) equipped with two neutral density polarizers and utilizing a 20-mesh wire screen. The sun is not a point source; however, the width of the diffraction tails was still considerably narrower than the sun diameter. Some improvements would accrue if atmospheric effects were not present.

The advent of semiconductor electron multiplier components for use in image dissector camera tubes has increased the flexibility of multi-aperture tubes of this type. A one-lens sub tracker capable of providing separate X and Y error signals could be developed using a three-aperture image dissector tube as shown in circuit to acquire the sun. Apertures P and Y, located well out on the diffraction tails, could be used to obtain separate X and Y error signals. An even simpler system could be developed with a lens, filter, and three photodiodes.

The main advantage of such a tracker is in reducing of light intensity of the sun's image, and thus protecting the detectors. From Fig 5.2 it may appear that the observed narrower width for diffraction tails would provide higher resolution in detection. This is not true, however, since the narrowing is primarily due to the attenuation of light energy in the tails and not due to energy compression in a smaller width by the 20-mesh wire screen. In other words the screen does not provide any energy compression.

## 5.4 Simulation Cross-Correlation

The simulation system of Fig. 4-1 was used with the laser, 350mm objective lens and apodization filter of Fig. 5-1a to obtain a photographic negative on Panatomic-X film of the cross-type diffraction pattern. After developing, the negative was mounted in a three-micrometer XYZ positioner and reinserted into the film plane for the XYZ positioner. The other components of the system shown in Fig. 4-1 were not moved during this experiment.

The purpose of this experiment was to obtain, as nearly as

possible, an autocorrelation of the cross-type diffraction pattern with itself. This experiment will be referred to as a cross-correlation rather than autocorrelation experiment because the film did not provide entirely linear reproduction of the signal. The film nonlinearities were minimized by using a low laser intensity and inserting three neutral density filters between the collimater lens and the filter throughout the experiment. The combined effect of the neutral density filters was to reduce the intensity by a factor of 200.

The cross-type diffraction pattern was the opaque portion of the film negative. Hence, maximum correlation occurred when a minimum amount of light energy passed through the negative. This energy was recorded by using the Exa camera with a 100mm lens. The entire experimental simulator consisted of the laser, diverger lens, pinhole, collimater lens, three neutral density filters, apodization filter with circular aperture ( Fig. 5-1a), 350mm objective lens, negative mounted on XYZ positioner, 100mm lens, and Exa camera.

Since it was not possible to move the simulated star, the same effect was obtained by moving the negative with the XYZ positioner. The negative was positioned in the focal plane of the 350mm objective lens at all times. The movement consisted of horizontal and vertical translation in a plane perpendicular to the optical axis. It was calculated that a 0.001-inch translation on the bench corresponded to an angular attitude error for the space craft of 15 seconds of arc. Figure 5-4 shows the results of translations along one of the diffraction tails which correspond to attitude errors of 15 seconds, 1 minute, and 4 minutes, respectively.

The camera used to take the pictures in Fig. 5-4 was then replaced with a 900-line scan vidicon television camera. By using the delayed sweep feature of a Tektronic 545 oscilloscope, the waveforms of individual scan lines could be observed. In other words, for the light intensity patterns shown in Fig. 5-4, translations of the reference pattern of 0.001 inch could easily be detected on the oscilloscope screen.

It should be noted that the aperture diameter of the pre-processing filter was 0.542.

## 5.5 General Conclusions

1. A wire screen placed in front of or behind the objective lens of a star tracker system would cause each star in the field of view to cast a cross-type diffraction pattern on a sensor

Fig. 5-4--Laser Cross-Correlation

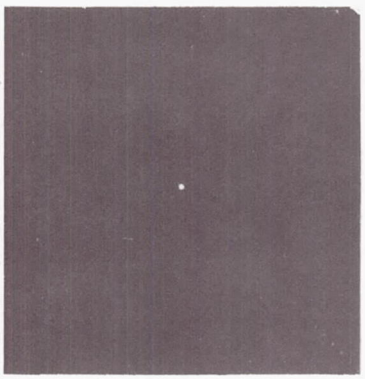

(a)
Alligned

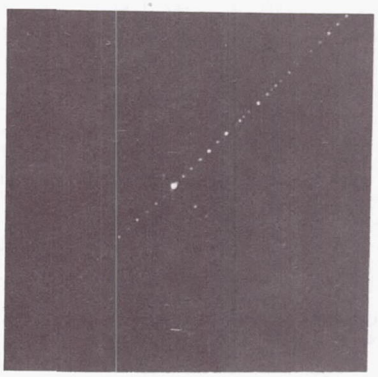

(b)
15 Arc-Seconds

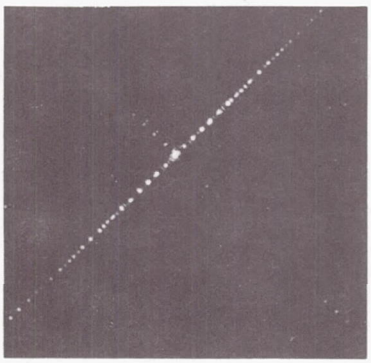

(c)
1 Minute

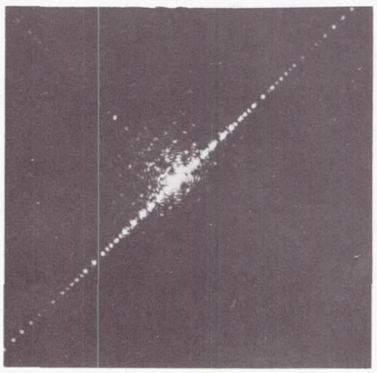

(d)
4 Minutes

placed in the focal plane of the objective lens.

2. Many of the nulls in this diffraction pattern may be removed by using wires of different diameteres in the wire screen filter. Only two different diameteres were used in this simulation. After observing stars with binoculars and simple screen filters it is felt that the use of wires with several different diameters would be useful in a real star-tracker system.

3. An undesirable spreading effect occurs when too many wires are used in the filter. The spreading effect depends upon the total number of wires in the filter and is not dependent upon whether or not there is an equal number of wires in both directions.

4. The main advantage of the cross-type diffraction approach is the separation of X and Y error signals without using moving parts in the tracker. Another advantage is the possibility of obtaining many samples of the X and Y positions in a single raster scan.

5. The cross-type diffraction approach provides a means of improving upon existing sun-tracker systems. Separation of X and Y errors are feasible, and the detectors can be protected from burning.

6. It would be possible to improve the signal-to-noise ratio of energy in the diffraction tails at the expense of tail length by moving the filter to the sensor side of the lens. The closer the filter is placed to the sensor, the larger the signal-to-noise ratio and the shorter the tails.

7. A 15 arc-second error signal could be detected with the 350mm lens and a 0.542-inch aperture used in the simulation.

# VI. DISCRETE SEQUENTIAL ESTIMATION OF THE IMAGE POSITION

## 6.1 Introduction

The purpose of the present discussion is development of a simple discrete electronic method of sequential estimation of coordinates of a number of stars in the image plane. This method requires a certain number of simple digital computations to be carried out by the small computer on board. The proposed method is briefly as follows: the star image intensity ( corrupted by sensor noise) is measured at a pre-specified ( or learned) finite number of points. From these noisy measurements the coordinates of the star in question are sequentially estimated. The advantages of such a method are as follows:

1. The storage requirements of the data necessary for carrying out the computations are minimal.

2. The computations are primarily linear operations.

3. The system is flexible so that, at the expense of more computations, faster results are obtainable, or accuracy can be increased, or both.

4. The system can be instructed to learn to proceed in making an optional sequence of measurements or any other measurement sequence necessitated by other constraints and limitations.

For simplicity, the discussion here is restricted to sequential estimation of the position of one star. The case where positions of several stars must be sequentially or simultaneously estimated is not treated here since that case is an extension of the one-star case.

First a procedure for estimating the coordinates of one star is developed, based on a finite number of measurements. This development is possible because the optical field can be pre-filtered, according to the methods of Part II, to render a star intensity $\Phi(u,v)$ of a particular shape.

Then a method of generalized mean square error minimization is presented for estimating the position of the star relative to a coordinate system.

## 6.2 Discrete Estimation of the Star Position

We assume the known intensity of the star image is $\Phi(u,v)$ in the two-dimensional image focal plane; and the orthogonal axes u and v are fixed in this plane with respect to the telescope. The sensor or scanner noise--$n(u,v)$--is assumed to be stationary with mean zero and is not correlated spatially from one point $(u_1, v_1)$ to another point $(u_2, v_2)$ in the image field. If the telescope is perfectly oriented, the signal observed is

$$\Phi(u,v) + k(u,v).$$

To this must be added the background noise $B(u,v)$. In the development that follows, it is assumed that $B(u,v)$ is constant[3] so that it does not enter into the computations.

If the telescope is not oriented perfectly, the signal observed is

$$\Phi(u+a, v+b) + k(u,v) = S. \qquad (6.1)$$

From successive observations of S at known points $(u_1, v_1)$, $(u_2, v_2)$, etc., a and b must be estimated. A further assumption is made here; i.e., during the estimation of a and b the telescope does not change its orientation. In other words, a and b are constants to be estimated from measurements of S at a number of points.

By pre-filtering the starfield according to the method of Part II, $\Phi(u,v)$ will be shaped such that in its Taylor series expansion in u and v only terms up to second-order dominate;

$$\Phi(u,v) = \Phi(o,o) + u\frac{\partial \Phi}{\partial u}\Big|_{o,o} + v\frac{\partial \Phi}{\partial v}\Big|_{o,o}$$
$$+\frac{u^2 \partial^2 \Phi}{2! \partial u^2}\Big|_{o,o} + uv\frac{\partial^2 \Phi}{\partial u \partial v}\Big|_{o,o} + \frac{v^2 \partial^2 \Phi}{2! \partial v^2}\Big|_{o,o} \qquad (6.2)$$

This is not an unreasonable restriction on $\Phi(u,v)$ since the main portion of the energy of the image is contained in its central hump which can very well be pre-filtered to render expansion Eq. (6.2).

Since $\Phi(u,v)$ is symmetric with respect to the axes u and v; namely, $\Phi(u,v) = \Phi(-u,v) = \Phi(u,-v)$, it follows that

$$\frac{\partial \Phi}{\partial u}\Big|_{0,0} = \frac{\partial \Phi}{\partial v}\Big|_{0,0} = 0. \qquad (6.3)$$

By the same argument, the star field can be pre-filtered to render an image that contains also the fourth-order terms $u^4$, $v^4$, and $u^2v^2$.

For the present we assume that Eq. (6.2) describes the image intensity. Letting the second derivatives be

$$\frac{1}{2}\frac{\partial^2 \Phi}{\partial u^2} = M$$

$$\frac{1}{2}\frac{\partial^2 \Phi}{\partial u \partial v} = J,$$

$$\frac{1}{2}\frac{\alpha^2 \Phi}{\alpha v^2} = L,$$

Eq. (6.2) becomes

$$\Phi(u,v) = \Phi(0,0) + Mu^2 + 2Juv + Lv^2 \qquad (6.4)$$

or

$$\Phi(u+a, v+b) = (Mu^2 + 2Juv + Lv^2) +$$

$$\Phi(0,0) + 2(uM + Jv)a + 2(vL + Ju)b +$$

$$Ma^2 + 2Jab + Lb^2. \qquad (6.5)$$

Now suppose S is measured at a number of points with specified coordinates $(u_1, v_1)$, $(u_2, v_2)$, etc. One then obtains the following sequence of equations:

At point 1

$$c_{11}a + c_{12}b + c_{13}a^2 + c_{14}ab + c_{15}b^2 = r_1, \qquad (6.6)$$

where

$$c_{11} = 2(u_1 M + J v_1),$$

$$c_{12} = 2(v_1 L + J u_1),$$

$$c_{13} = M,$$

$$c_{14} = 2J,$$

$$c_{15} = L,$$

and $r_1$ is a random variable,

$$r_1 = s_1 - \Phi(0,0) - M u_1^2 - 2J u_1 v_1 - L v_1^2 - k_1(u,v).$$

At point 2

$$c_{21} a + c_{22} b + c_{23} a^2 + c_{24} ab + c_{25} b^2 = r_2, \qquad (6.7)$$

at point 3

$$c_{31} a + c_{32} b + c_{33} a^2 + c_{34} ab + c_{35} b^2 = r_3, \qquad (6.8)$$

and so forth.

We can assume that a, b, $a^2$, ab, and $b^2$ are five independent variables and solve the sequence of linear equations above to derive the best estimates $\hat{a}$, $\hat{b}$, $\hat{a^2}$, $\hat{ab}$, and $\hat{b^2}$.

Two separate cases will be considered; i.e., (1) there are fewer equations than unknowns, and (2) there are more equations than unknowns. The first case may occur where an estimate is necessary after every measurement.

## 6.3 Generalized Mean Square Error Minimization

The criterion considered here is generalized mean square minimization. Let the matrix of coefficient $c_{ij}$ be designated by C; let the m variables be estimated from a column vector A (here m=5); let the number of equations be n ($n < m$); and let the known n vector on the right side be R. Then the following system of equations must be solved for A:

$$CA = R, \qquad (6.9)$$

where R is the column vector

$$\begin{matrix} r_1 \\ r_2 \\ r_3 \\ \cdot \\ \cdot \\ \cdot \\ r_n \end{matrix}$$

We define two additional vectors that are necessary later; i.e., the random noise vector

$$K = \begin{matrix} k_1\ (u_1, v_1) \\ k_2\ (u_2, v_2) \\ \cdot \\ \cdot \\ k_n\ (u_n, v_n) \end{matrix}$$

and

$$T = \begin{matrix} s_1 - \Phi(0,0) - Mu_1^2 - 2Ju_1v_1 - Lv_1^2 \\ s_2 - \Phi(0,0) - Mu_2^2 - 2Ju_2v_2 - Lv_2^2 \\ \cdot \\ \cdot \\ s_n - \Phi(0,0) - Mu_n^2 - 2Ju_nv_n - Lv_n^2 \end{matrix} .$$

It is obvious that

$$R = K + T.$$

Equation ( 6.9) is solved subject to minimization of a generalized norm for vector A;

$$I_1 = \frac{1}{2} A^T Q A, \qquad (6.10)$$

where $I_1$ is a scalar and Q is a specified positive definite matrix ( alternately Q can be derived through learning procedures).

Minimization of I subject to the constant Eq. ( 6.9) renders

$$A = Q^{-1}C^T(CQ^{-1}C^T)^{-1}R. \qquad (6.11)$$

This estimation requires inversion of a matrix $CQ^{-1}C^T$ every time a measurement is added. If the estimate is necessary prior to the time m measurements are taken, these inverses can be a priori computed and stored. If one can wait until at least m measurements are taken, one can proceed with system (6.9) again. However, now $n > m$; namely, there are more equations than unknowns. Selection of a performance index

$$I_2 = \frac{1}{2}(CA - R)^T Q(CA - R), \qquad (6.12)$$

when Q is a positive n x n matrix and minimizing its subject to constraint, Eq. (6.9) renders

$$\hat{A} = (C^TQC)^{-1} C^TQR. \qquad (6.13)$$

When n measurements are taken

$$\hat{A}_n = (C_n^TQ_nC_n)^{-1} C_n^TQ_nR_n; \qquad (6.14)$$

when n + 1 measurements are taken

$$\hat{A}_{n+1} = (C_{n+1}^TQ_{n+1}C_{n+1})^{-1} C_{n+1}^TQ_{n+1}R_{n+1}. \qquad (6.15)$$

This estimation has two primarily computational limitations; i.e., matrices Q of successively higher and higher dimension must be stored; and, for every n, a matrix $C_n^TQ_nC_n$ must be inverted. To circumvent these two limitations, we assume Q = I--the identity matrix. Thus

$$\hat{A}_{n+1} = (C_{n+1}^TC_{n+1})^{-1} C_{n+1}^TR_{n+1}. \qquad (6.16)$$

Thus the storage of matrices Q is no longer necessary. If the problem of inverting $C_{n+1}^T C_{n+1}$ can be achieved in a simple manner, then Eq. (6.16) is practical from a computational point of view. Actually $C_{n+1}^T C_{n+1}$ can be inverted in a simple manner and the result of this inversion is the development of a recursive formula for $\hat{A}_{n+1}$ in terms of $\hat{A}_n$ and the latest measurement $r_{n+1}$, and the parameters of matrix C, i.e., $c_{(n+1)1}, c_{(n+1)2}, \ldots c_{(n+1)m}$ associated with the $n^{th}$ point where the signal is measured. This development is followed below utilizing a known formula[4] for matrix inversion.

Let the row vector $c_{(n+1)1}, c_{(n+1)2}, \ldots c_{(n+1)m}$ be designated by $\beta$;

$$C_{n+1} = \frac{C_n}{\beta}, \qquad (6.17)$$

then

$$C_{n+1}^T C_{n+1} = C_n^T C_n + \beta^T \beta. \qquad (6.18)$$

Using the inversion formula cited above

$$(C_{n+1}^T C_{n+1})^{-1} =$$

$$(C_n^T C_n)^{-1} \{I - \beta^T [1 + \beta (C_n^T C_n)^{-1} \beta^T]^{-1} \beta (C_n^T C_n)^{-1}\}. \qquad (6.19)$$

By utilizing Eqs. (6.19) and (6.18) in Eq. (6.16) one obtains

$$\hat{A}_{n+1} = \hat{A}_n + (C_n^T C_n)^{-1} \beta^T [1 + \beta (C_n^T C_n)^{-1} \beta^T]^{-1} [r_{n+1} - \beta \hat{A}_n]. \qquad (6.20)$$

Thus $\hat{A}_{n+1}$ is a function of $\hat{A}_n$--the immediate former estimate, $\beta$; the latest observation $r_{n+1}$; and finally $(C_n^T C_n)^{-1}$ that has already been computed. The only inversion in Eqs. (6.20) and (6.19) is the inversion of a scalar quantity, $1 + \beta (C_n^T C_n)^{-1} \beta^T$.

This generalized mean square error technique requires knowledge of an initial estimate $\hat{A}_0$. Either, through trial and error, good initial estimates can be guessed at, or from the first m measurements an estimate $\hat{A}_m$ is computed (by solving m equations in m unknowns). From that point on the recursive formula Eq. (6.20) is applied.

## 6.4 Implications of the Recursive Estimation Technique

A desirable feature of this technique is that $\hat{a}$ and $\hat{a^2}$, and $\hat{b}$ and $\hat{b^2}$ are simultaneously estimated after every measurement. This permits computation of the quantities $(\hat{a})^2 - (\hat{a^2})$ and $(\hat{b})^2 - (\hat{b^2})$ which can be used as a measure of how good the estimates are, and when these quantities are decreased to acceptable values the recursion can be stopped. A second advantage of this technique is that it can be adapted to fewer computations. If the measurements as two successive points are subtracted, the difference is a linear equation in a and b only and does not contain the nonlinear terms $a^2$, $b^2$, and ab;

$$\Phi(u_1+a,\ v_1+b) - \Phi(u_2+a,\ v_2+b) =$$

$$[(u_1-u_2)M + (v_1-v_2)N]\,a + [(v_1-v_2)L + (u_1-u_2)N]\,b$$

$$+ M(u_1^2-u_2^2) + 2N(u_1v_1-u_2v_2) + L(u_1^2-u_1^2-u_2^2). \qquad (6.21)$$

Thus one can estimate only $\hat{a}$ and $\hat{b}$ recursively.

A third advantage of this technique is its flexibility for repeating the measurements at a fixed set of points, or at an arbitrary set of points in the image plane.

If the set of points is fixed, the signal at such points can be picked up by photocells or other small sensors at such points and a vidicon or image orthicon is not necessary.

The main disadvantage of this technique is that the error in position (namely, a and b) must be within the main hump of the star image.

The covariance of the error in estimating vector A can be computed. If this covariance tends to zero as the number n of measurements is increased, the estimates $\hat{a}$, $\hat{b}$, $\hat{a^2}$, $\hat{b^2}$, etc. converge to the true values a, b, $a^2$, $b^2$, etc. This covariance can be computed as follows: consider the case where $n>m$. If the noise K were zero, A would be the solution of

$$CA = T, \qquad (6.22)$$

where $\hat{A}$ is the solution of

$$C\hat{A} = R. \qquad (6.23)$$

From Eq. (6.22)

$$A = (C^TC)^{-1}C^TT.$$

From Eq. (6.23)

$$\hat{A} = (C^TC)^{-1}C^TR,$$

or the error vector

$$\hat{e} = A-\hat{A} = (C^TC)^{-1}\,C^TK.$$

The error covariance is the m x m matrix

$$P_n = \overline{e_n e_n^T} = \overline{(C_n^T C_n)^{-1} C_n^T K_n K_n^T C_n (C_n^T C_n)^{-1}}.$$

Since the noise is assumed to be spatially and temporally uncorrelated,

$$KK^T = \sigma^2 I_n,$$

where $\sigma^2$ is the standard deviation of the noise and $I_n$ is the identy matrix

$$P_n = \sigma^2 (C_n^T C_n)^{-1}. \qquad (6.24)$$

Similarly

$$P_{n+1} = \sigma^2 (C_{n+1}^T C_{n+1})^{-1}. \qquad (6.25)$$

Thus, making use of Eq. (6.19),

$$P_{n+1} = P_n - P_n \beta^T (\sigma^2 + \beta P_n \beta^T)^{-1} \beta P_n. \qquad (6.26)$$

In Eq. (6.26) the three m x m matrices, $P_{n+1}$, $P_n$ and $P_n \beta^T (\sigma^2 + \beta P_n \beta^T)^{-1} \beta P_n$, are all positive definite, and $P_{n+1}$ will tend to zero as n increases. This is analogous to the case where from a positive scalon quantity $\gamma_n$ another positive scalar quantity proportional to $\gamma_n$ is subtracted, and the difference (namely, $\gamma_{n+1}$) is positive. The limit of $\gamma_n$ as n increases is equal to zero.

# VII. DISCRETE ESTIMATION USING THE CROSS PATTERN

## 7.1 Introduction

The previous parts have described two basically different methods for estimating alignment errors in the star image position. The first is optical analog cross-correlation and the second is discrete linear sequential estimation by a computer. Both of these methods suffer from shortcomings, however. The cross-correlation method, as described, is not readily extendable to the case of multiple star patterns. Furthermore, cross-correlation methods generally require the storage of correlation masks. The mask must be changed whenever a new pattern is used for alignment, and the problems of precisely positioning the new mask by an automatic mechanical system may be severe. Furthermore, this system is not readily adaptable to the pattern recognition and location task which is a necessary prerequisite to pattern alignment.

The discrete sequential estimation procedure described in the previous part is very attractive because of its generality and flexibility and because the necessary hardware could also be used for pattern recognition and location. However this system requires that the functional form of the image intensity be precisely known for each star. In theory this is not prohibitive but in practice it may be a difficult requirement to fulfill for several reasons. First, the shape of the intensity function depends not only on the form of the image-shaping filter used but, as shown in Part II, also on the spectral density function of the star's light output. This varies widely from star to star and so the system would need to know the image intensity function of each individual star. Furthermore the response of photodetectors varies from unit to unit and for a single unit may vary with such factors as temperature and age.

For these reasons an entirely different approach has been sought which would overcome the shortcomings of the methods previously examined. Preliminary system requirements have been set as follows:

1. The system must work for multiple star patterns.

2. There must be no moving mechanical parts.

3. There must be a minimum requirement for knowledge of the image intensity functions.

4. The system must be easily adaptable to different patterns.

5. The same hardware must be usable for pattern recognition purposes.

This part describes a design for such a system. The general approach is described, after which some aspects of the functional form of the image intensity are discussed. It is then shown that part of the system can be realized digitally and that multiple star patterns are easily processed by the system. The desirability of a cross-shaped star image is demonstrated, and the effects of system noise are considered. Finally the adaptability of the system to pattern recognition is shown.

## 7.2 General Approach to the System

If the satellite is in its desired orientation, the telescope and any optical filters used in conjunction with it will cast an image of some star or stars on a plane behind the optical system. The light intensity of this image can be denoted as a function $\Phi(u,v)$ measured on an arbitrary coordinate system in the image plane. Concentrating for the present on the case of a single star, a small error in the orientation of the satellite will result in an image intensity $\Phi(u+a, v+b)$. In order to drive the craft back to its proper alignment, the errors a and b must be determined. Presented with this problem in a completely abstract setting, one might begin by computing the mean values of u and v weighted by $\Phi(u+a, v+b)$ as one finds the mean of a probability density function. This leads, for u, to the integral

$$\int_{-\infty}^{\infty} u\Phi(u+a, v+b)\,du. \qquad (7.1)$$

Making the substitution u+a=w, the expression becomes

$$\int_{-\infty}^{\infty} (w-a)\Phi(w, v+b)\,dw, \qquad (7.2)$$

or

$$\int_{-\infty}^{\infty} w\Phi(w, v+b)\,dw - a\int_{-\infty}^{\infty} \Phi(w, v+b)\,dw. \tag{7.3}$$

If $\Phi(u,v)$ is even in u[ i.e. $\Phi(u,v) = \Phi(-u,v)$ ], the first integral in Eq. (7.3) will vanish. In this case setting (7.3) equal to (7.1) and replacing w by u + a results in an expression for a;

$$a = -\frac{\int_{-\infty}^{\infty} u\Phi(u+a, v+b)\,du}{\int_{-\infty}^{\infty} \Phi(u+a, v+b)\,du}. \tag{7.4}$$

If $\Phi(u,v)$ is also even in v a similar expression gives the value of b.

A method for determining the alignment errors begins to emerge. In Fig. 7-1a a set of equal intensity contours of a possible $\Phi(u,v)$ projected onto the u-v plane is shown. Figure 7-1b shows the contours of $\Phi(u+a, v+b)$ resulting from a small displacement of the image.

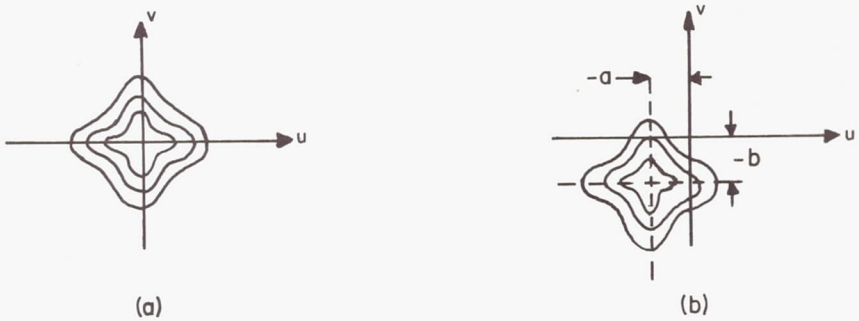


Fig. 7-1--Star Images: (a) centered, (b) displaced.

Equation (7-4) shows that the integration on u may be taken at any value of v and similarly for those on v. Since, for small displacements, the image center is always near the origin, it is sensible to choose to integrate along the u and v axes. Then **a** and **b** are

$$a = - \frac{\int_{-\infty}^{\infty} u \Phi(u+a, b)\, du}{\int_{-\infty}^{\infty} \Phi(u+a, b)\, du} \tag{7.5}$$

and

$$b = - \frac{\int_{-\infty}^{\infty} v \Phi(a, v+b)\, dv}{\int_{-\infty}^{\infty} \Phi(a, v+b)\, dv} . \tag{7.6}$$

In an actual system, $\Phi(u+a, b)$ and $\Phi(a, v+b)$ could be generated by scanning the proper lines in the image plane with an image dissector or similar sensor.

## 7.3 Evenness of Image Intensity Function

An important point in the development of this approach is that the requirements of evenness on $\Phi(u, v)$ can be met. In this section it is shown that this can be accomplished by choosing a complex amplitude transmission function for the optical system which has the same type of evenness as $\Phi(u, v)$.

From the results of Part II, $\Phi(u, v)$ can be written as

$$\Phi(u, v) = \int_0^{\infty} \theta(w) \Phi_w(u, v)\, dw, \tag{7.7}$$

where

$$\Phi_w(u, v) = \int_{-\infty}^{\infty}\int \phi(\Delta_1, \Delta_2)\, e^{-j(w/cf)(\Delta_1 u + \Delta_2 v)}\, d\Delta_1\, d\Delta_2 \tag{7.8}$$

and

$$\phi(\Delta_1, \Delta_2) = \int_{-\infty}^{\infty}\int f(x+\Delta_1, y+\Delta_2) f^*(x, y)\, dxdy; \tag{7.9}$$

and where

$\theta(w)$ = Temporal Energy Spectrum of Source,

$f(x,y)$ = Complex Amplitude Transmission Function of Optical System, and

$\Phi_w(u,v)$ = Image Intensity Due to Monochromatic Source of Frequency w.

Now if $f(x,y)$ is chosen so that

$$f(x,y) = f(-x,y), \tag{7.10}$$

then

$$\phi(\Delta_1, \Delta_2) = \int_{-\infty}^{\infty}\int f(-x-\Delta_1, y+\Delta_1) f^*(-x, y)\, dxdy; \tag{7.11}$$

and letting $z = -x$,

$$\phi(\Delta_1, \Delta_2) = \int_{-\infty}^{\infty}\int f(z-\Delta_1, y+\Delta_2)\, f^*(z, y)\, dzdy$$

$$= \phi(-\Delta_1, \Delta_2). \tag{7.12}$$

Using this result in Eq. (7.8) with a similar change of variable shows that

$$\Phi_w(u,v) = \Phi_w(-u,v). \tag{7.13}$$

Thus it follows immediately from Eq. (7.7) that

$$\Phi(u,v) = \Phi(-u,v). \tag{7.14}$$

A similar procedure can be carried out for v. The final result is that an image which satisfies

$$\Phi(u,v) = \Phi(-u,v) = \Phi(u,-v) \tag{7.15}$$

can be obtained by using an optical transmission function which satisfies

$$f(x,y) = f(-x,y) = f(x,-y). \tag{7.16}$$

This is not a difficult requirement to fulfill.

## 7.4 Digital Realization of the System

Calculation of a and b by analog means presents considerable circuit problems from both accuracy and reliability standpoints. By using analog to digital conversion and a small special purpose computer these problems can be circumvented. Digital forms of Equations (7.5) and (7.6) can be written by using the sampling theorem which states that a function f(t) whose Fourier transform F(w) is zero outside the interval (-W, W) can be written as

$$f(t) = \sum_{n=-\infty}^{\infty} f_n \frac{\sin(Wt-n\pi)}{Wt-n\pi},$$

where $f_n$ are samples of f(t);

$$f_n = f\left(n\frac{\pi}{W}\right).$$

Since $\Phi(u,v)$ is an image formed by an optical system of finite aperture, its Fourier transform is zero outside some interval, and the same is true of $\Phi(a, v+b)$ and $\Phi(u+a, b)$, so the sampling theorem may be applied to them. Following this argument it is easy to show that Eqs. (7.5) and (7.6) may be rewritten exactly as

$$a = -\frac{\pi}{B} \frac{\sum_{n=-\infty}^{\infty} n\Phi_{nu}}{\sum_{n=-\infty}^{\infty} \Phi_{nu}} \tag{7.17}$$

and

$$b = -\frac{\pi}{B} \frac{\sum_{n=-\infty}^{\infty} n\Phi_{nv}}{\sum_{n=-\infty}^{\infty} \Phi_{nv}}, \tag{7.18}$$

where B is the bandwidth of $\Phi(a, v+b)$ and $\Phi(u+a, b)$ and where $\Phi_{nu}$ and $\Phi_{nv}$ are samples of these signals;

$$\Phi_{nu} = \Phi\left(n\frac{\pi}{B} + a, b\right) \tag{7.19}$$

and

$$\Phi_{nv} = \Phi\left(a, n\frac{\pi}{B} + b\right). \tag{7.20}$$

In an actual system it is to be expected that $\Phi(a, v+b)$ and $\Phi(u+a, b)$ will be negligible small outside some reasonable interval. So to a good approximation, Eqs. (7.17) and (7.18) may be written as

$$a = -\frac{\pi}{B}\,\frac{\sum_{n=-N}^{N} n\Phi_{nu}}{\sum_{n=-N}^{N} \Phi_{nu}} \tag{7.21}$$

$$b = -\frac{\pi}{B}\,\frac{\sum_{n=-N}^{N} n\Phi_{nv}}{\sum_{n=-N}^{N}} \tag{7.22}$$

These equations can be made particularly accurate by choosing the proper form for $\Phi(u, v)$, as will be discussed later.

## 7.5 Shape of the Star Image

So far, little has been said about the particular shape of the star image intensity pattern $\Phi(u, v)$. It has been noted that it must be even in u and in v, but what other characteristics should it have? For the detection scheme described here to work in its simplest form, the displaced image $\Phi(u+a, v+b)$ of each star must overlap a pair of perpendicular lines through the point at which the image would be centered when properly aligned. This suggests that the image should be as large as possible so that even for large alignment errors this overlapping criterion will be met. However, for a fixed aperture, the star image will have fixed evergy. If the star image is spread out over a large area, then the energy density in $w/cm^2$ will be low. If the photodetector has a threshold energy density below which no signal is detected, spreading out the image may result in making the star go completely unnoticed.

Thus one is presented with the seemingly irreconcilable requirements of maximum linear dimensions and minimum area. However, if one notes that the width in the u direction need be large only at one value of v and vice versa, a solution is apparent. An image in the shape of a cross can have very little area and still have large linear dimensions in

the u and v directions. A cross can also have the required symmetry about the u and v axes. The synthesis of an optical filter which will produce a cross image is discussed elsewhere in the report.

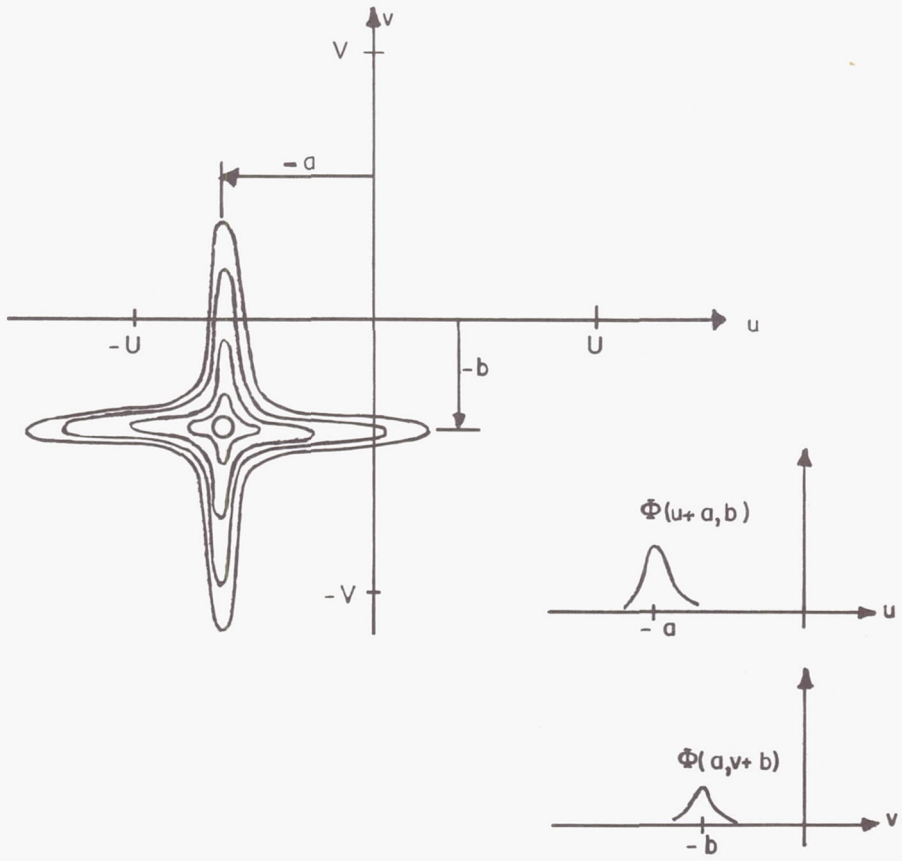


Fig. 7-2 --Displaced Star Image and Resulting Scanner Output

Figure 7-2 shows equi-intensity contours projected onto the u-v plane for a possible cross form of $\Phi(u+a, v+b)$. Also shown are the resulting form of $\Phi(u+a, b)$ and $\Phi(a, v+b)$. It can be seen that for this configuration Eqs. (7.21) and (7.22), whose summation limits are finite, will be quite accurate if the scans along the u and v axes are reasonably long, say between U and -U and between V and -V, as shown in Fig. 7-2.

## 7.6 Multiple Star Case

If the system is to be used for stabilizing a space craft, it must be able to determine three components of the craft's orientation

error: pitch, yaw, and roll. Assuming that the roll axis is taken as the optical axis of the detection system, pitch and yaw errors will cause apparent displacement of the star pattern in the U and V directions ( see Fig. 7-3) while roll errors will cause rotation of the pattern about the center of the coordinate system. Fig. 7-3 and the discussion below make it clear that only two stars are needed to determine all three components of the error provided the error is small. ( Assuming the system cannot distinguish between two different stars $S_1$ and $S_2$, then a roll error $\theta$ could not be distinguished from an error $\theta + \pi$. )

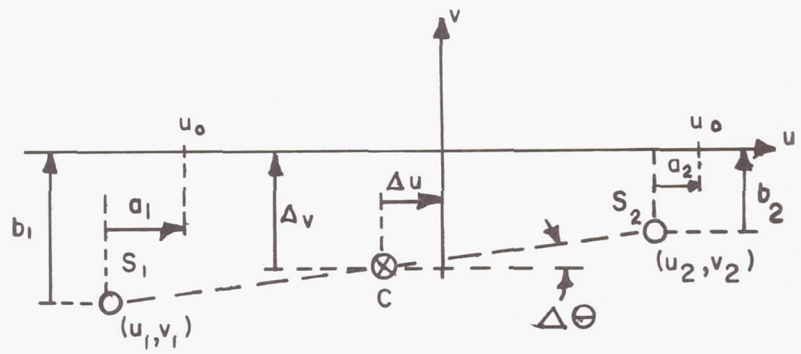


Fig. 7-3--A Misaligned Two-Star Pattern

As explained previously, the system determines the misalignment of a single star by scanning along a mutually perpendicular pair of lines centered at the point where the star image would be if the craft were properly aligned. Therefore, the system can easily handle multi-star patterns by scanning along a pair of lines for each star. For example, in Fig. 7-3 the pattern is properly aligned when the stars $S_1$ and $S_2$ have coordinates $( -u_{O2}, 0)$ and $( +u_o, 0)$ respectively. So the system would scan the lines $u = -u_o$, $u = +u_o$ and $v = o$. If the star images overlap these lines, as shown in Fig. 7-2, the system detects a and b for each star as follows:

$$a_1 = u_1 + u_o,$$
$$b_1 = v_1,$$
$$a_2 = u_2 - u_o, \text{ and}$$
$$b_2 = v_2$$

In this example, $a_1$, $b_1$, $a_2$ and $b_2$ are all negative numbers.

Measurement of these form quantities is sufficient for estimating roll, yaw and pitch as was mentioned before. In order to show this we observe that the misalignment of the two-star pattern has three components; i.e., two translational errors and one rotational error. These may be expressed as

$$\Delta u = \frac{u_1 + u_2}{2} = \frac{a_1 + a_2}{2} \qquad (7.23)$$

$$\Delta v = \frac{v_1 + v_2}{2} = \frac{b_1 + b_2}{2} \text{ , and} \qquad (7.24)$$

$$\Delta\theta = \arctan \frac{v_1 - v_2}{u_1 - u_2}$$

$$= \arctan \frac{b_2 - b_1}{a_2 - a_1 + 2u_o} \text{ .} \qquad (7.25)$$

$\Delta\theta$ is the roll error in the craft's alignment. The pitch and yaw errors can be directly calculated from $\Delta u$ and $\Delta v$ and the known geometry of the optical system.

For patterns with more than two stars, a similar procedure can be followed, or a pair of stars can be singled out from the rest and the above method used.

## 7.7 The Noisy Case

In this section an approximate analysis of the noisy case will be made.

In a real system the output of the scanner will not be deterministic. The signal $\Phi(a, v+b)$, for example, will not be available for determination of b. The available signal will be

$$S(v) = \Phi(a, v+b) + k(v), \qquad (7.26)$$

where $k(v)$ is random noise. Therefore b must be estimated. The estimation can be achieved by one scan, or by a number of scans. Referring to Fig. 7.2, all these scans will be taken along the v axis and have a length of 2v (from the point with coordinates 0, -V to the point with coordinates 0, V). First the case of one scan is discussed. Let the estimate of b from one single scan be $\hat{b}$, it is natural to calculate it by the formula

$$\hat{b} = -\frac{\pi}{B} \frac{\sum_{i=-N}^{N} i S_i}{\sum_{i=-N}^{N} S_i} \qquad (7.27)$$

where

$$S_i = S\left(i\frac{\pi}{B}\right)$$

$$= \Phi\left(a,\ i\frac{\pi}{B} + b\right) + k\left(i\frac{\pi}{B}\right)$$

$$= \Phi_{iv} + k_i. \qquad (7.28)$$

This estimate will be in error by an amount

$$\Delta b = \hat{b} - b.$$

Denoting the expectation operator by $E(\cdot)$, the mean of $\Delta b$ is

$$E(\Delta b) = E\left[-\frac{\pi}{B}\frac{\sum_{i=-N}^{N} i\Phi_{iv} + \sum_{i=-N}^{N} ik_i}{\sum_{i=-N}^{N}\Phi_{iv} + \sum_{i=-N}^{N} k_i}\right] - b\ . \qquad (7.29)$$

In general this expectation will be very difficult to calculate. However, if the noise has mean zero, the fact that the $\Phi_{iv}$'s are all positive makes it reasonable to assume that

$$\sum_{i=-N}^{N}\Phi_{iv} >> \sum_{i=-N}^{N} k_i. \qquad (7.30)$$

Then

$$E(\Delta b) \tilde{=} b - \frac{\pi}{B}\frac{E\left[\sum_{i=-N}^{N} ik_i\right]}{\sum_{i=-N}^{N}\Phi_{iv}} - b = 0. \qquad (7.31)$$

So the estimator is unbiased.

The variance will be

$$\mathrm{Var}(\Delta b) = E[(\hat{b}-b)^2] - E^2[\hat{b}-b]$$

$$= E(\hat{b}^2) - b^2$$

or

$$\mathrm{Var}(\Delta b) = E\left[\left(\frac{\pi}{B}\right)^2 \frac{\left(\sum_{i=-N}^{N} i\Phi_{iv} + \sum_{i=-N}^{N} ik_i\right)^2}{\sum_{i=-N}^{N} \Phi_{iv} + \sum_{i=-N}^{N} k_i}\right] - b^2 . \tag{7.32}$$

Again assuming inequality (7.30), this reduces to

$$\mathrm{Var}(\Delta b) = \left(\frac{\pi}{B}\right)^2 \frac{E\left(\sum_{i=-N}^{N} ik_i \sum_{i=-N}^{N} jk_j\right)}{\left(\sum_{i=-N}^{N} \Phi_{iv}\right)} . \tag{7.33}$$

Now some more specific assumptions about the nature of the noise are needed. Suppose the noise is white and that by means of low pass filtering the bandwidth of $k(v)$ is reduced to that of $\Phi(a, b+v)$ - namely $(-B, B)$. Then, approximately,

$$E(k_i k_j) = \begin{cases} \sigma^2 & ; \quad i = j \\ 0 & ; \quad i \neq j \end{cases} , \tag{7.34}$$

and then

$$\mathrm{Var}(\Delta b) \simeq \left(\frac{\pi}{B}\right)^2 \frac{\sigma^2 \sum_{i=-N}^{N} i^2}{\left(\sum_{i=-N}^{N} \Phi_{iv}\right)} \tag{7.35}$$

or

$$\text{Var } \Delta b = \left(\frac{\pi}{B}\right)^2 \frac{\sigma \quad N(N+1)(2N+1)}{3 \sum_{i=-N}^{N} \Phi_{iv}} \qquad (7.36)$$

For large N this is approximately

$$\text{Var}(\Delta b) = \left(\frac{\pi}{B}\right)^2 \frac{2\sigma^2 N^3}{3\left(\sum_{i=-N}^{N} \Phi_{iv}\right)^2} \qquad (7.37)$$

If the image plane is scanned between the limits $(-V, V)$ as shown in Fig. 7-2, then

$$V = N\frac{\pi}{B} . \qquad (7.38)$$

Also

$$\sum_{i=-N}^{N} \Phi_{iv} = \frac{B}{\pi} \int_{-V}^{V} \Phi(a, v+b)\, dv. \qquad (7.39)$$

So

$$\text{Var}(\Delta b) = \frac{\pi}{B} \frac{2\sigma^2 V^3}{3\left(\int_{-V}^{V} \Phi(a, v+b)\, dv\right)^2} \qquad (7.40)$$

Several comments are pertinent here to the one scan case. According to Eq. (7.40) the length 2 V should be short for reducing the variance of $\Delta b$, and consequently increasing the accuracy of the one scan estimate. Also examination of Fig. 7.2 shows that as a becomes small, the denominator of Eq. 7.40 increases, and the variance of $\Delta b$ decreases. This means the system is more sensitive for smaller errors in alignment, and consequently small errors can be more accurately detected.

If one scan does not provide a good estimate, a number of scans can provide a better estimate. All these scans would be taken sequentially at the same spot. If M scans are taken, the estimate is the average of the M individual estimates; and, since each scan is statistically independent of the previous ones (because the noises of successive scans are independent), the variance of error for M scans is reduced by a factor of $\frac{1}{M}$.

If the system is to work for large values of b, V must also be large and so the variance of the estimates is deteriorated. This suggests that perhaps other methods of estimating b would be superior. In the literature of radar, methods for optimum estimation of pulse positions have been developed; however, these methods require that the functional form of the pulse be known. As explained in Section 7.1, any such method seems to be impractical for a star tracker operating on more than one star. Thus it would appear that research on methods for optimum pulse location estimation with limited knowledge about the waveform of the pulse would have great value for star-tracker applications.

## 7.8 Using the System for Pattern Recognition

When the space vehicle reaches its proper orbit it may be in some random unknown orientation. Before the attitude control task begins the craft must be properly oriented. To do this the initial orientation must be determined so that appropriate corrections can be made. This requires pattern recognition.

For purposes of pattern recognition the coordinates of the stars in the field need not be determined with great precision since all that is necessary is to avoid confusing one pattern with another. Therefore, the hardware required for the attitude control system could be used in any of several different ways to recognize star patterns.

One simple scheme is to first scan the field of view horizontally in a conventional television raster and integrate each line of the scan. Those lines passing nearly over the center of a star will have large integrals compared with those which do not. For a particular star there may be two or more consecutive lines with large integrals, but since high precision is not necessary the line with the largest integral can be assumed to pass directly through the star's center. This horizontal scan will locate the y-coordinate of each star in the field. A similar vertical scan will locate each x-coordinate. At this point the reader may object that the method does not tell which y-coordinate goes with which x-coordinate. This is true, but it turns out that this information is not

required. To see why, a pattern of three stars may be considered.

The three stars may be thought of as forming a triangle. The lengths of the sides of this triangle are invariant under any translation or rotation of coordinates. Therefore the sum of the squares of these lengths is fixed, and so

$$[(x_1-x_2)^2+(y_1-y_2)^2]+[(x_1-x_3)^2+(y_1-y_3)^2]$$
$$+[(x_2-x_3)^2+(y_2-y_3)^2]=K, \qquad (7.41)$$

where the $i^{th}$ star has coordinates $(x_i, y_i)$ and K is a constant characteristic of the particular pattern. Simplification leads to

$$2\sum_{i=1}^{3}x_i^2+a\sum_{i=1}^{3}y_i^2-\sum_{\substack{i=1\\ i\neq j}}^{3}\sum_{j=1}^{3}x_ix_j-\sum_{\substack{i=1\\ i\neq j}}^{3}\sum_{j=1}^{3}y_iy_j=K. \qquad (7.42)$$

Examination of this equation shows that it is not necessary to know which $x_i$ go with which $y_i$. Having determined the $x_i$ and $y_i$, the system feeds them to a computer which sums the squares of the $x_i$ and the $y_i$ and subtracts all cross products of the $x_i$ and of the $y_i$. The resulting number is compared with those in a stored set. If the difference between the computed K and one of the stored K's is within some bound, the pattern is considered recognized.

For N stars the equation generalizes to

$$(N-1)\sum_{i=1}^{N}x_i^2+(N-1)\sum_{i=1}^{N}y_i^2-\sum_{\substack{i=1\\ i\neq j}}^{N}\sum_{j=1}^{N}x_ix_j-\sum_{\substack{i=1\\ i\neq j}}^{N}\sum_{j=1}^{N}y_iy_j=K. \qquad (7.43)$$

Equation (7.43) can be justified by the following argument:

Join each of the N stars to every other star. Then the sum of the squares of the lengths of the lines joining the stars equals some constant K. Now consider the line joining the $i^{th}$ and $j^{th}$ stars. The square of its length is given by

$$L_{ij}^2=(x_i-x_j)^2+(y_i-y_j)^2=x_i^2+x_j^2+y_i^2+y_j^2-2x_ix_j-2y_iy_j \qquad (7.44)$$

Taking the sum of these squares

$$\frac{1}{2}\sum_{\substack{i=1\\ i\neq j}}^{N}\sum_{j=1}^{N} L_{ij}^{2} = K. \tag{7.45}$$

The factor 1/2 is introduced since each line is counted twice in the double summation, once as $L_{mn}$ and once as $L_{nm}$. Equation (7.45) can be expanded by means of Eq. (7.44) as follows:

$$\frac{1}{2}\sum_{\substack{i=1\\ i\neq j}}^{N}\sum_{j=1}^{N} L_{ij}^{2} = \frac{1}{2}\sum_{\substack{i=1\\ i\neq j}}^{N}\sum_{j=1}^{N}(x_i^2 + x_j^2) +$$

$$\frac{1}{2}\sum_{\substack{i=1\\ i\neq j}}^{N}\sum_{j=1}^{N}(y_i^2 + y_j^2) -$$

$$\frac{1}{2}\sum_{\substack{i=1\\ i\neq j}}^{N}\sum_{j=1}^{N} 2x_iy_i - \frac{1}{2}\sum_{\substack{i=1\\ i\neq j}}^{N}\sum_{j=1}^{N} 2y_iy_j. \tag{7.46}$$

The first part of Eq. (7.46) is

$$\frac{1}{2}\sum_{\substack{i=1\\ i\neq j}}^{N}\sum_{j=1}^{N}(x_i^2 + y_i^2) = [(x_1^2 + x_2^2) + (x_1^2 + x_3^2) + (x_1^2 + x_4^2)$$

$$+ \cdots + (x_1^2 + x_N^2)] +$$

$$[(x_2^2 + x_1^2) + (x_2^2 + x_3^2) + \cdots + (x_2^2 + x_N^2)] +$$

$$\cdots + [(x_N^2 + x_1^2) + (x_N^2 + x_2^2) + \cdots + (x_N^2 + x_{N-1}^2)] . \tag{7.47}$$

Now $x_1^2$ occurs (N-1) times between the first set of brackets and one time between each of the remaining (N-1) sets of brackets. The same thing is true for the other $x_i$. Therefore,

$$\frac{1}{2} \sum_{\substack{i=1 \\ i \neq j}}^{N} \sum_{j=1}^{N} (x_i^2 + x_j^2) = \frac{2(N-1)}{2} \sum_{i=1}^{N} x_i^2 .$$

Applying the same argument to the $y_i$, Eq. (7.46) may be rewritten in the form of Eq. (7.43).

Other methods of determining the coordinates of the stars may be used; but, regardless of the method, it can be seen that the hardware necessary for attitude control can also be used for pattern recognition.

## 7.9 Conclusions

This part has outlined the design for a system which meets the five general requirements listed in Section 7.1. The brief noise calculations in Section 7.7, however, suggest that if a requirement for high accuracy and a requirement that the system work for fairly large misalignments are added, the system may fail to meet both of them simultaneously. Considerable additional analysis would be necessary to resolve this question.

## REFERENCES


1. Packard, J. N., "Electro-Optical Image Matches for Space Guidance Applications," IEEE Transactions on Aerospace and Navigational Electronics, ANE-10, No. 3, pp. 282-289, September 1963.

2. Born, M. and Wolfe, E., Principles of Optics, The Macmillan Company, New York 1964, pp. 393-404.

3. Foudriat, E.C., "Application of Maximum Likelihood Techniques to the Design of Optimum Star Trackers," NASA Technical Note, NASA TND-4549, May 1968.

4. Sain M.K., "On a Useful Matrix Inversion Formula and Its Applications," Proceedings of IEEE, Vol. 55, No. 10, p. 1753, October 1967.




NASA-Langley, 1969 —— 21 CR-1443